# Bottomonium suppression in the QGP

## From EFTs to non-unitary quantum evolution

Michael Strickland
Kent State University
Kent, OH USA

N. Brambilla, M.-A. Escobedo, A. Islam, MS, A. Tiwari, A. Vairo, P. Vander Griend,
2205.10289, JHEP 2022, 303
and references therein

Excited QCD
Sicily, Italy
October 28, 2022

KENT STATE UNIVERSITY
U.S. DEPARTMENT OF ENERGY
TUM Global
Ohio Supercomputer Center
An OH·TECH Consortium Member

# Bottomonium Suppression

- In a high temperature quark-gluon plasma we expect **weaker color binding** (Debye screening)

  T. Matsui and H. Satz, Phys. Lett. B178, 416 (1986)
  F. Karsch, M. T. Mehr, and H. Satz, Z. Phys. C37, 617 (1988)

- Also, high energy plasma particles which slam into the bound states cause them to have shorter lifetimes → **large spectral widths**

  M. Laine, O. Philipsen, P. Romatschke, and M. Tassler, JHEP 03, 054 (2007)

TUMQCD Collaboration, 1804.10600

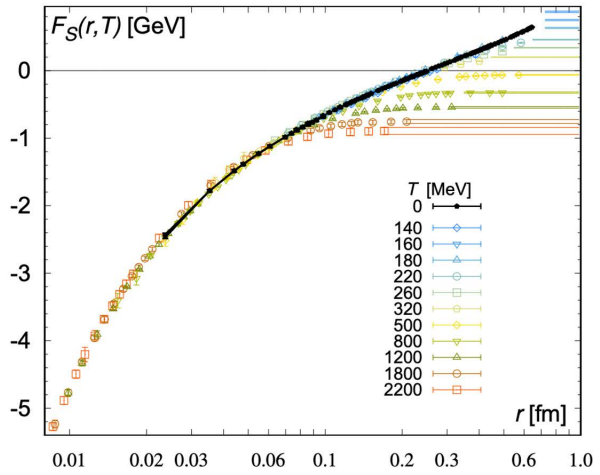


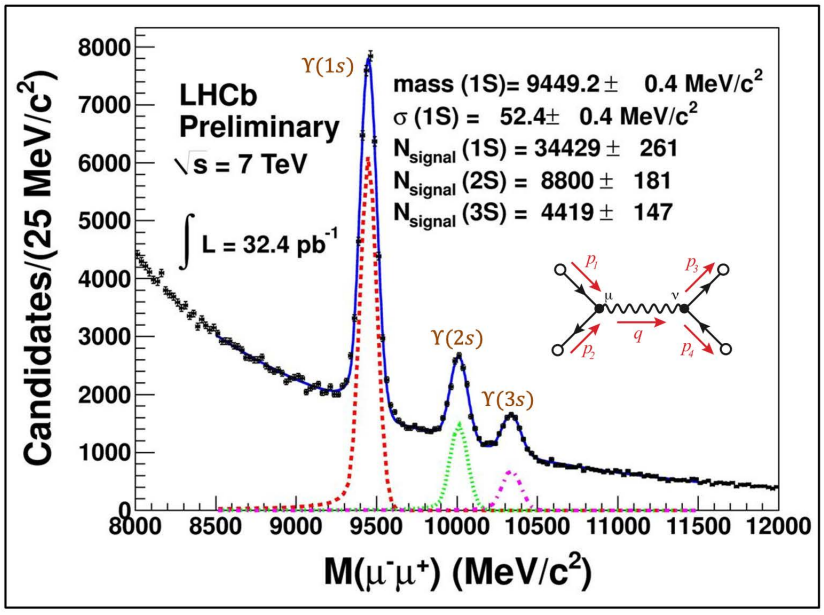


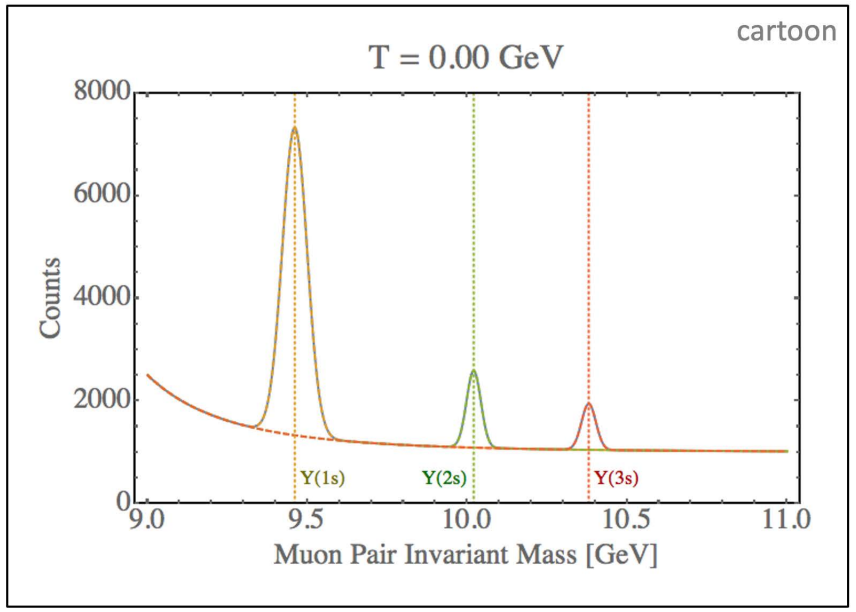

# Debye-screening in a plasma

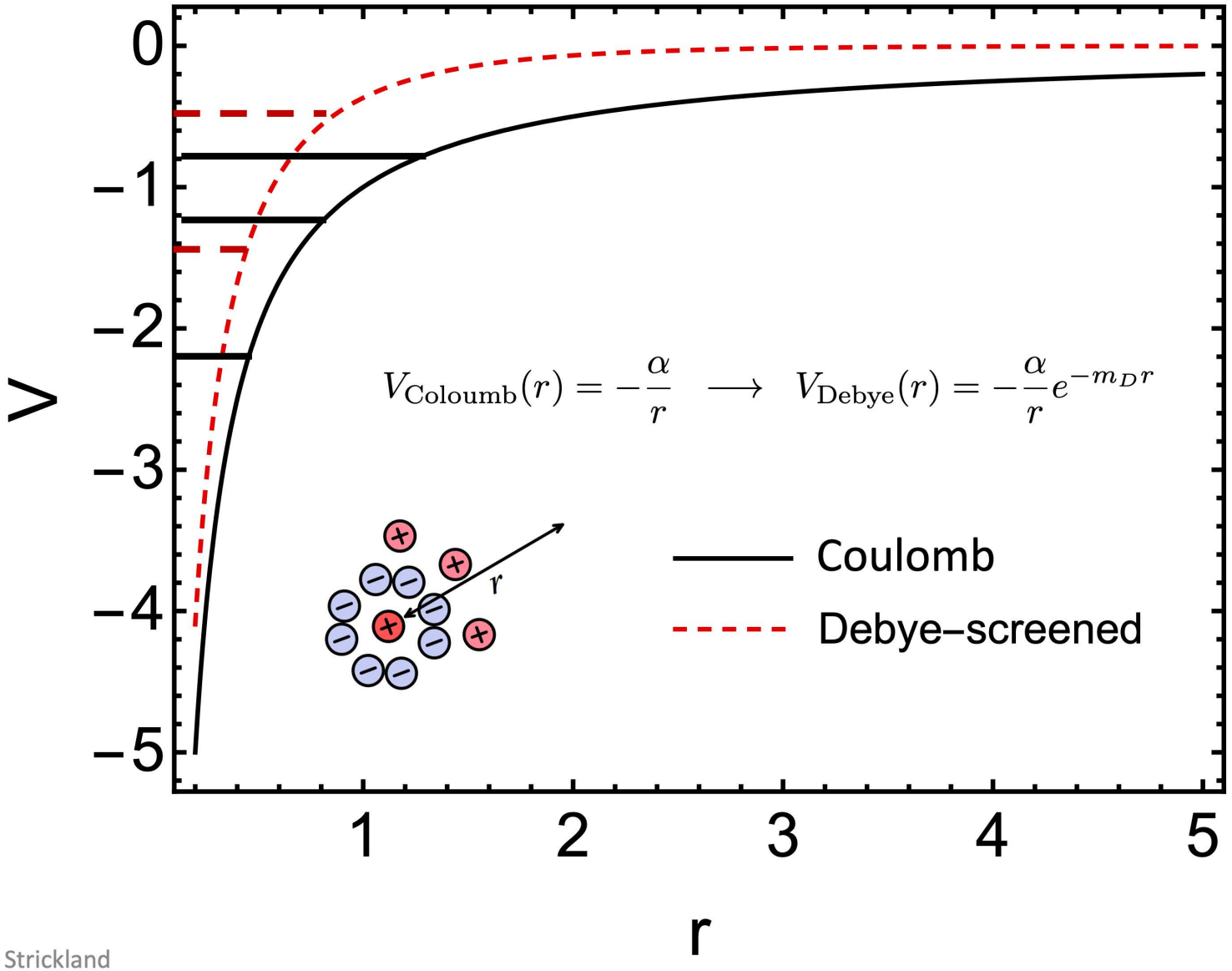


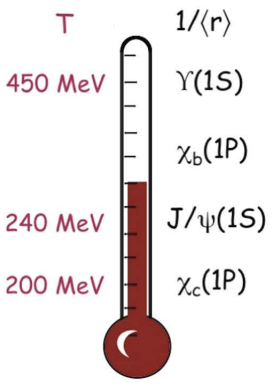


A. Mocsy, P. Petreczky, and MS, 1302.2180

# Bottomonium Suppression

- In a high temperature quark-gluon plasma we expect **weaker color binding** (Debye screening)

  T. Matsui and H. Satz, Phys. Lett. B178, 416 (1986)
  F. Karsch, M. T. Mehr, and H. Satz, Z. Phys. C37, 617 (1988)

- Also, high energy plasma particles which slam into the bound states cause them to have shorter lifetimes → **large spectral widths**

  M. Laine, O. Philipsen, P. Romatschke, and M. Tassler, JHEP 03, 054 (2007)

TUMQCD Collaboration, 1804.10600

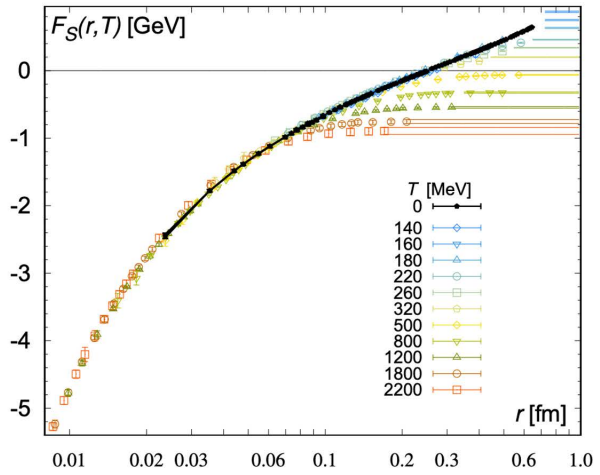


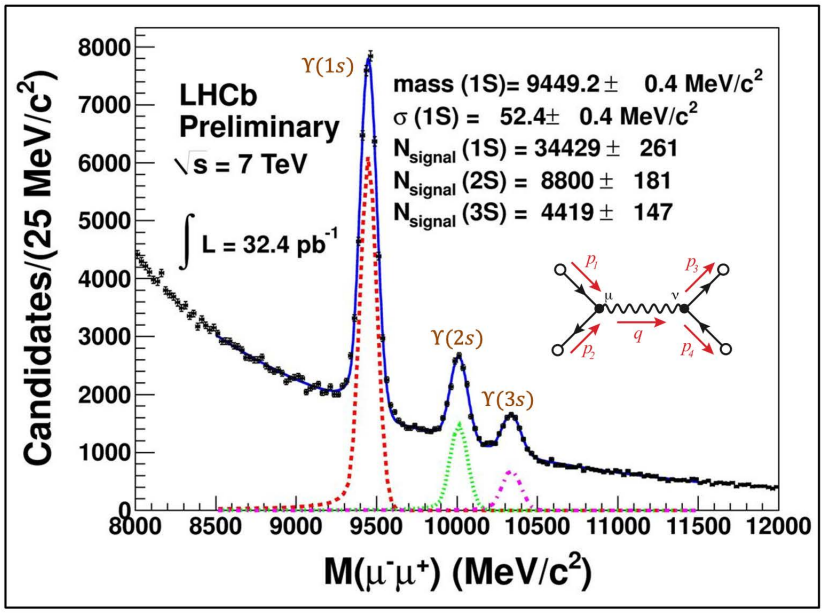


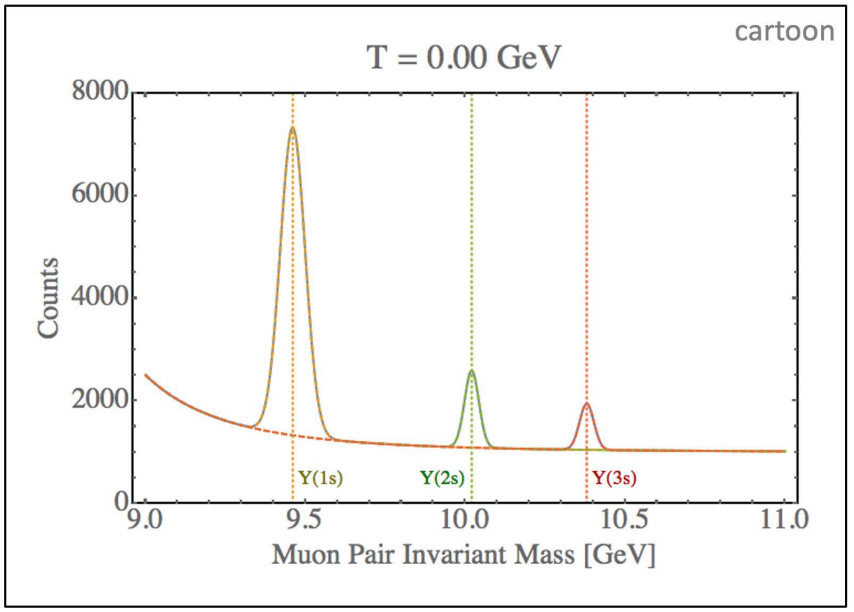

# Bottomonium Suppression

- In a high temperature quark-gluon plasma we expect **weaker color binding** (Debye screening)

  T. Matsui and H. Satz, Phys. Lett. B178, 416 (1986)
  F. Karsch, M. T. Mehr, and H. Satz, Z. Phys. C37, 617 (1988)

- Also, high energy plasma particles which slam into the bound states cause them to have shorter lifetimes → **large spectral widths**

  M. Laine, O. Philipsen, P. Romatschke, and M. Tassler, JHEP 03, 054 (2007)

TUMQCD Collaboration, 1804.10600

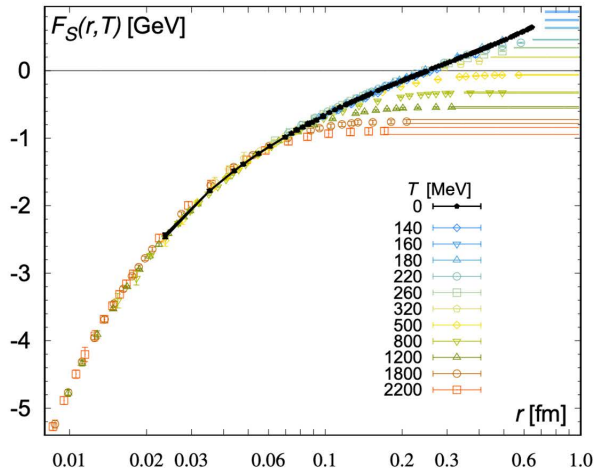


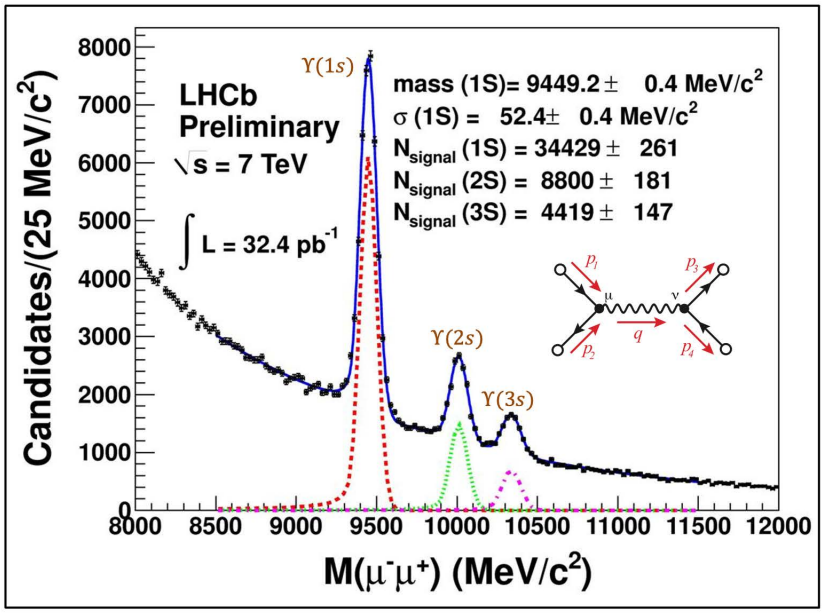


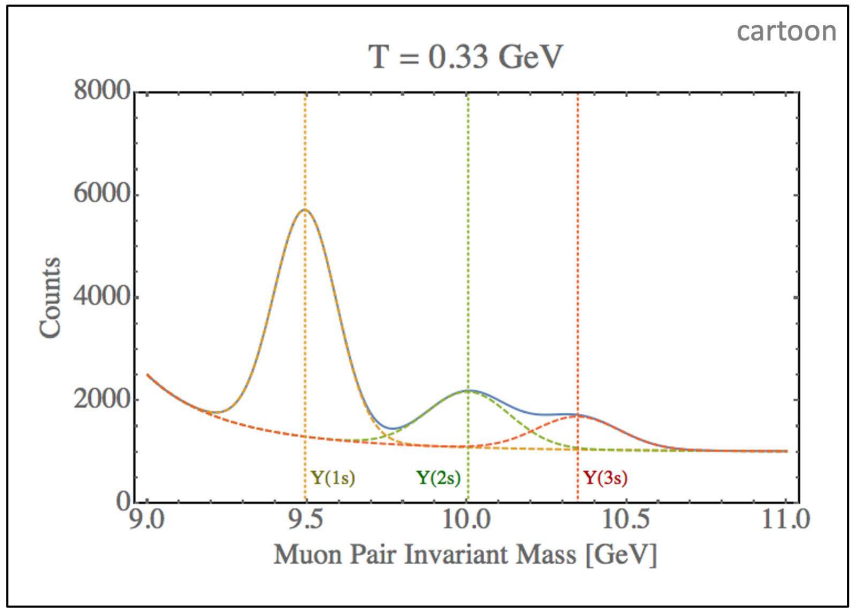

# Bottomonium Suppression

- In a high temperature quark-gluon plasma we expect **weaker color binding** (Debye screening)

  T. Matsui and H. Satz, Phys. Lett. B178, 416 (1986)
  F. Karsch, M. T. Mehr, and H. Satz, Z. Phys. C37, 617 (1988)

- Also, high energy plasma particles which slam into the bound states cause them to have shorter lifetimes → **large spectral widths**

  M. Laine, O. Philipsen, P. Romatschke, and M. Tassler, JHEP 03, 054 (2007)

TUMQCD Collaboration, 1804.10600

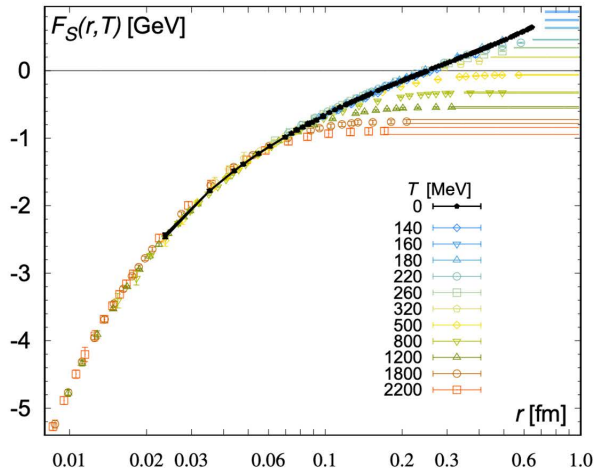


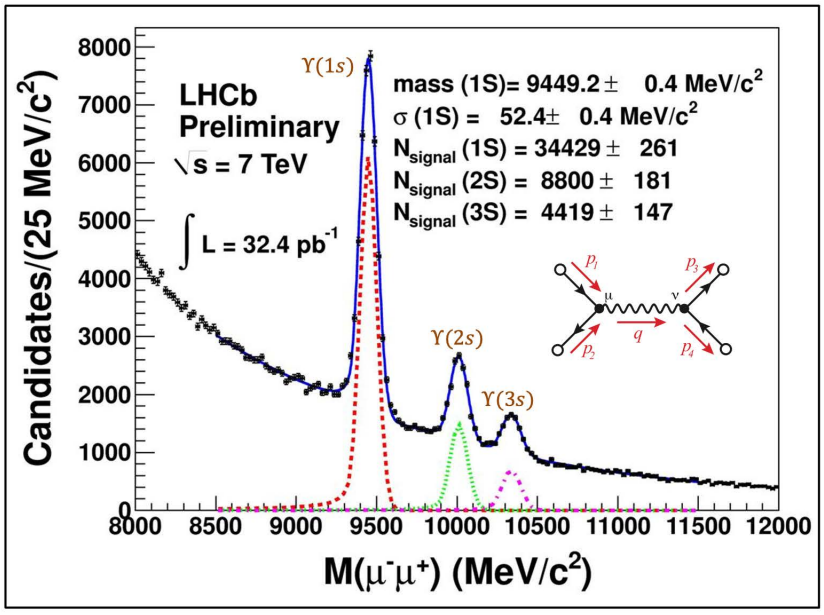


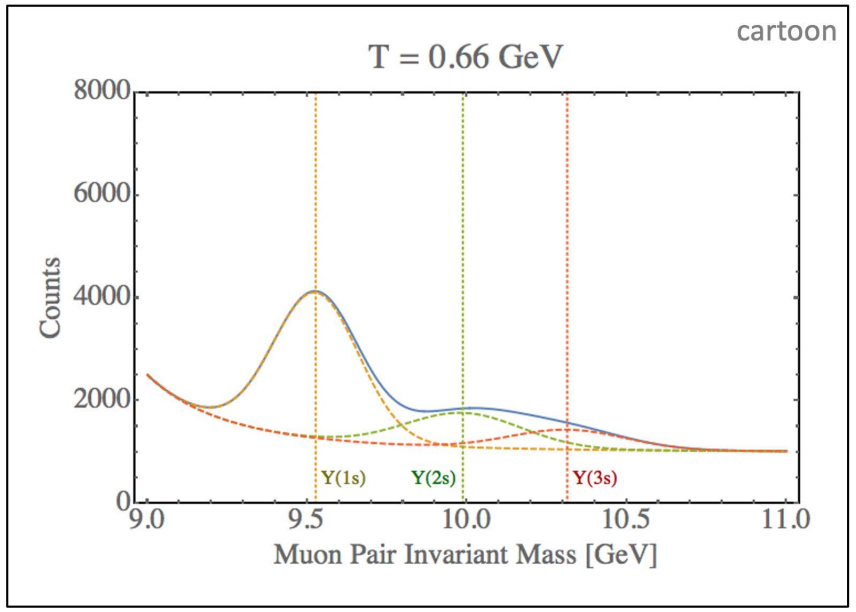

# Bottomonium Suppression

- In a high temperature quark-gluon plasma we expect **weaker color binding** (Debye screening)

  T. Matsui and H. Satz, Phys. Lett. B178, 416 (1986)
  F. Karsch, M. T. Mehr, and H. Satz, Z. Phys. C37, 617 (1988)

- Also, high energy plasma particles which slam into the bound states cause them to have shorter lifetimes → **large spectral widths**

  M. Laine, O. Philipsen, P. Romatschke, and M. Tassler, JHEP 03, 054 (2007)

TUMQCD Collaboration, 1804.10600

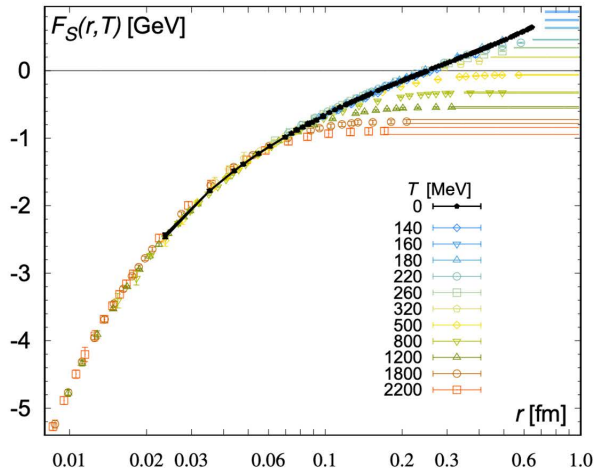


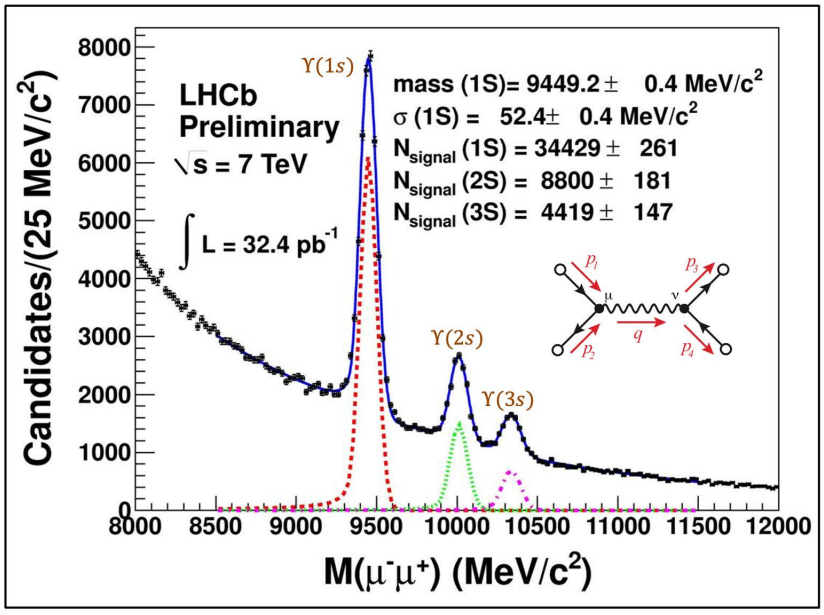


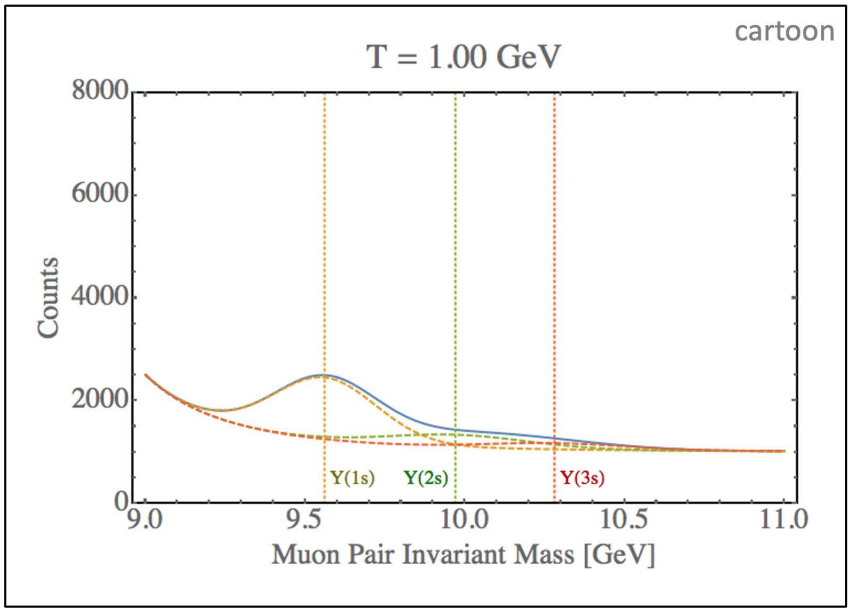

# Experimental data – 5.02 TeV Dimuon Spectra

The **CMS, ALICE,** and **ATLAS** experiments have measured bottomonium production in both pp and Pb-Pb collisions at 5.02 TeV. Here, I show CMS results.

**pp**

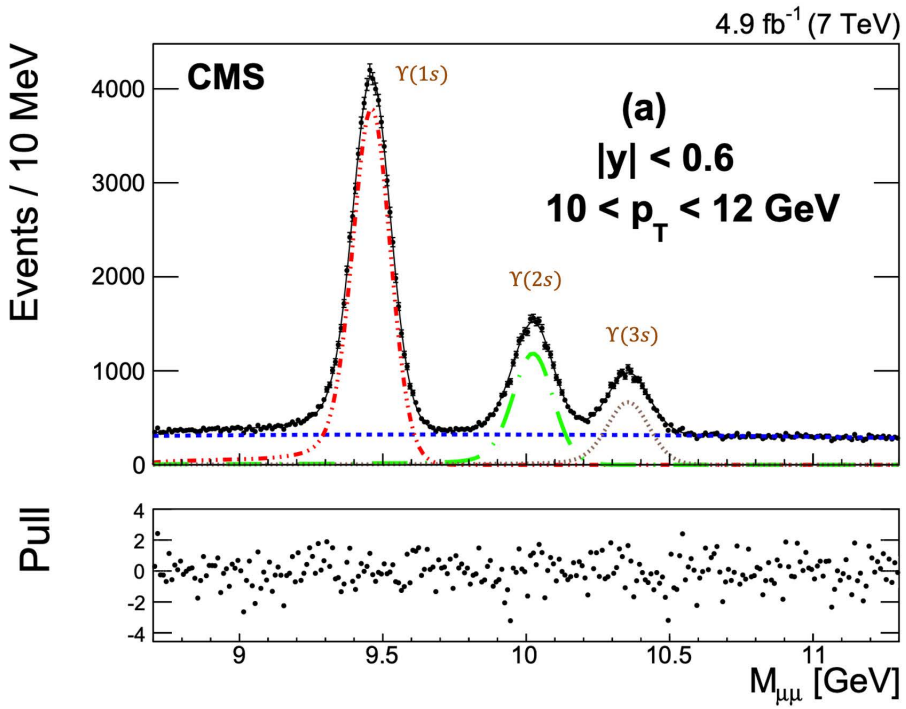


**PbPb**

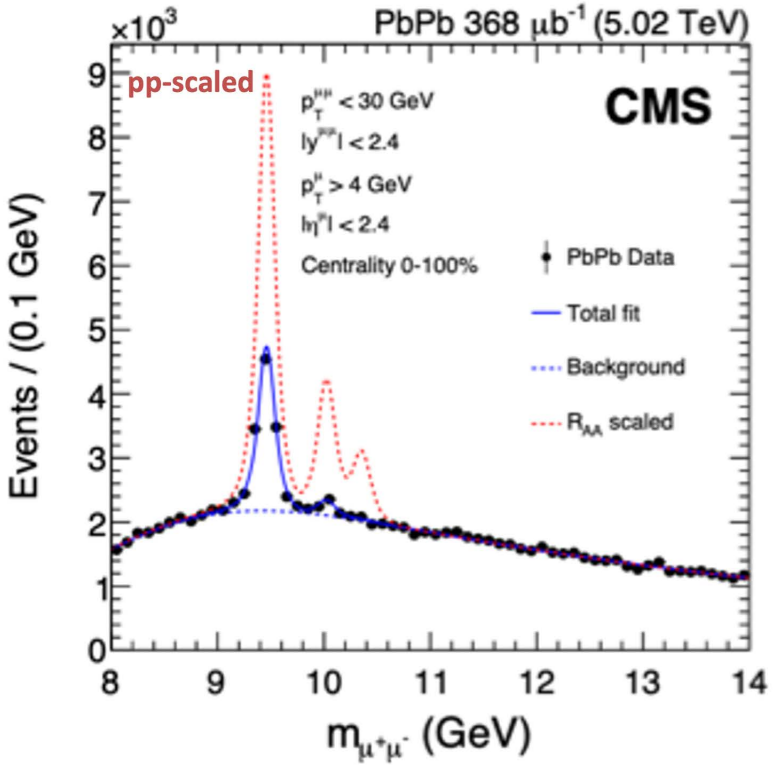

# Conceptual problem

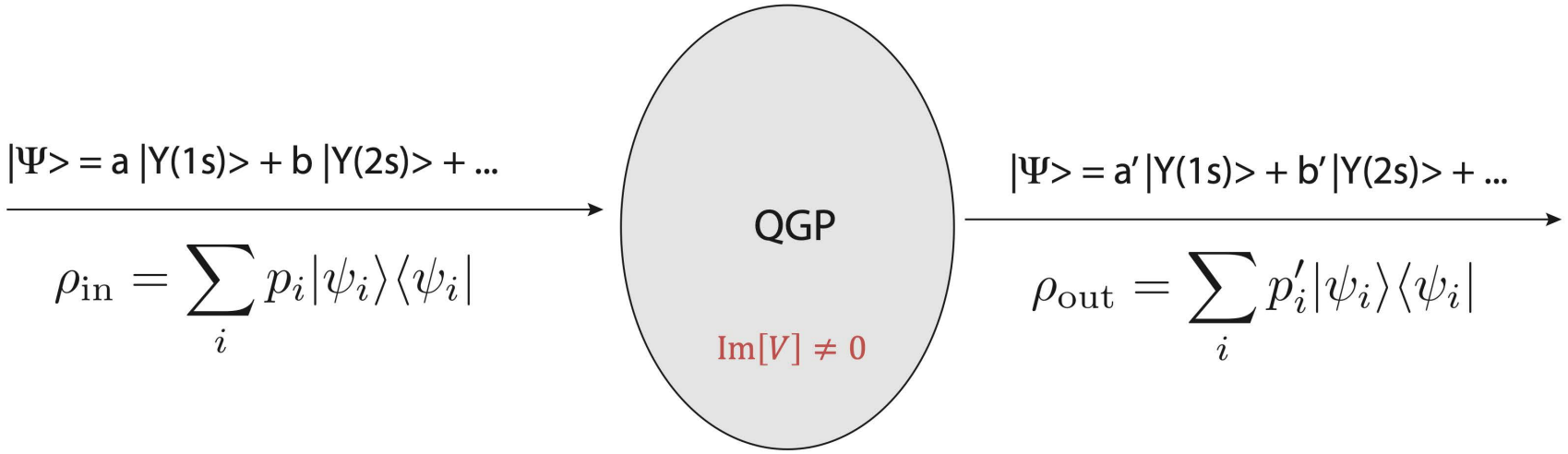


- Bottomonium states are produced locally (hard processes) at early times in hard collisions (t < 1 fm/c).
- They then propagate through the plasma and interact with the medium.
- Bound states can break up and potentially re-form due to in-medium transitions induced by in-medium gluon absorption and emission.

# Open quantum system (OQS) approach

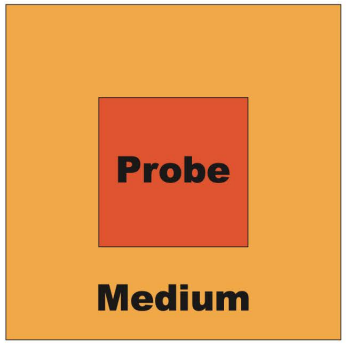


**Probe** = heavy-quarkonium state

**Medium** = light quarks and gluons that comprise the QGP

- Can treat heavy quarkonium states propagating through QGP using an open quantum system approach

$$H_{\rm tot} = H_{\rm probe} \otimes I_{\rm medium} + I_{\rm probe} \otimes H_{\rm medium} + H_{\rm int}$$

- Total density matrix

$$\rho_{\rm tot} = \sum_j p_j |\psi_j\rangle\langle\psi_j| \quad \longrightarrow \quad \frac{d}{dt}\rho_{\rm tot} = -i[H_{\rm tot}, \rho_{\rm tot}]$$

- Reduced density matrix (medium DOF integrated out)

$$\rho_{\rm probe} = {\rm Tr}_{\rm medium}[\rho_{\rm tot}] \quad \longrightarrow \quad \textbf{“Master equation”}$$

# OQS + pNRQCD → Lindblad equation

- What are the relevant scales?
  - Temperature $T$
  - Bound state mass $m \gg T$
  - Bound state size $r \sim 1/mv \sim a_0$ (Bohr radius)
  - Debye mass $m_D$
  - Binding energy $E \sim mv^2$

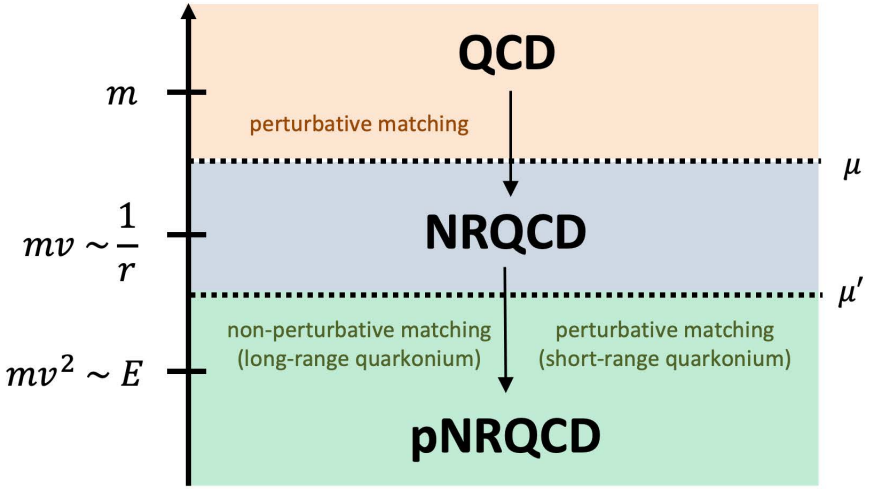


- Separation of time scales
  - Medium relaxation time scale $\langle \hat{O}_{\rm M}(t)\hat{O}_{\rm M}(0)\rangle \sim e^{-t/t_{\rm M}} \to \frac{1}{T}$
  - Intrinsic probe time scale $t_P \sim \frac{1}{\omega_i - \omega_j} \to \frac{1}{E}$
  - Probe relaxation time scale $\langle p(t)\rangle \sim e^{-t/t_{\rm rel}} \to \frac{1}{\text{self-energy}} \sim \frac{1}{\alpha_s a_0^2 \Lambda^3}$ $\quad \Lambda = T, E$

$$1/r \gg T \sim m_D \gg E \xrightarrow[t_{\rm rel}\,,\; t_{\rm P} \gg t_{\rm M}]{}$$

$$\frac{d\rho_{\rm probe}}{dt} = -i[H_{\rm probe}, \rho_{\rm probe}] + \sum_n \left( C_n\, \rho_{\rm probe}\, C_n^\dagger - \frac{1}{2}\{C_n^\dagger C_n, \rho_{\rm probe}\} \right)$$

N. Brambilla, M. A. Escobedo, J. Soto and A. Vairo, 1612.07248, 1711.04515

# OQS + pNRQCD – Lindblad reorganization

$$\frac{d\rho_{\rm probe}}{dt} = -i[H_{\rm probe}, \rho_{\rm probe}] + \sum_n \left( C_n \, \rho_{\rm probe} \, C_n^\dagger - \frac{1}{2}\{C_n^\dagger C_n, \rho_{\rm probe}\} \right)$$

- $H_{\rm probe}$ is Hermitian (includes singlet and octet states)
- $C_n$ are the **collapse (or jump) operators** (connect different internal states)
- Partial and **total decay width operators** are

$$\Gamma_n = C_n^\dagger C_n \qquad \Gamma = \sum_n \Gamma_n$$

- Can reorganize Lindblad equation by defining

$$H_{\rm eff} = H_{\rm probe} - \frac{i}{2}\Gamma$$

← **Non-Hermitian effective Hamiltonian**

$$\longrightarrow \quad \frac{d\rho_{\rm probe}}{dt} = -iH_{\rm eff}\rho_{\rm probe} + i\rho_{\rm probe}H_{\rm eff}^\dagger + \sum_n C_n \, \rho_{\rm probe} \, C_n^\dagger$$

# Potential NRQCD (pNRQCD)

Pineda and Soto, '97; Brambilla, Pineda, Soto, and Vairo '99, '00, '03

$$\mathcal{L} = -\frac{1}{4} F^a_{\mu\nu} F^{\mu\nu,a} + \mathrm{Tr}\left\{ S^\dagger \left( i\partial_0 - \frac{\mathbf{p}^2}{m} - V_s \right) S + O^\dagger \left( i\partial_0 - \frac{\mathbf{p}^2}{m} - V_o \right) O \right\}$$

$$+ V_A \,\mathrm{Tr}\left\{ O^\dagger\, \mathbf{r}\cdot g\mathbf{E}\, S + S^\dagger\, \mathbf{r}\cdot g\mathbf{E}\, O \right\} \rightarrow$$

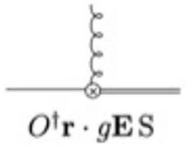


$$+ \frac{V_B}{2} \mathrm{Tr}\left\{ O^\dagger\, \mathbf{r}\cdot g\mathbf{E}\, O + O^\dagger O\, \mathbf{r}\cdot g\mathbf{E} \right\} \rightarrow$$

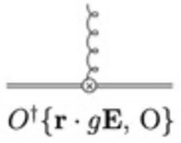


**Singlet and octet potentials**

$$V_s(r) = -C_F \frac{\alpha_s}{r}$$

$$V_o(r) = \frac{\alpha_s}{2N_c r}$$

- Based on this Lagrangian, we can perform first-principles calculations.
- Right figure shows diagrams contributing to singlet and octet self-energies.
- These enter into the calculation of Lindblad/collapse/jump operators.

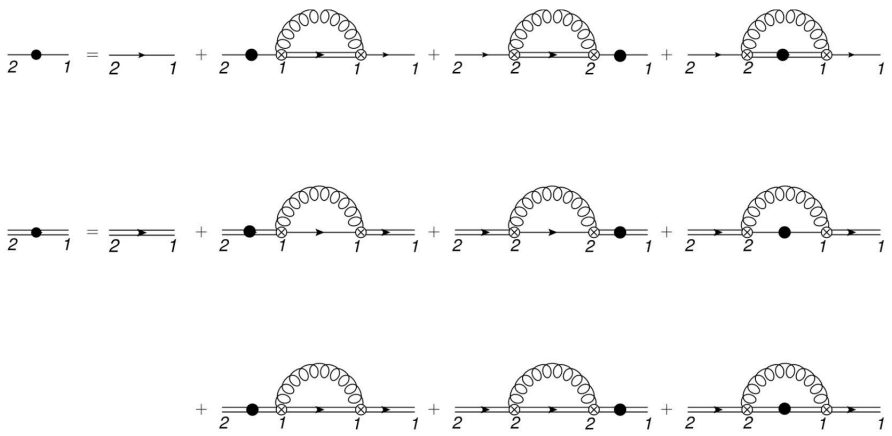

# LO OQS + pNRQCD Hamiltonian and collapse operators

N. Brambilla, M. A. Escobedo, J. Soto and A. Vairo, 1612.07248, 1711.04515

$$\frac{d\rho_{\rm probe}}{dt} = -iH_{\rm eff}\rho_{\rm probe} + i\rho_{\rm probe}H_{\rm eff}^\dagger + \sum_n C_n\,\rho_{\rm probe}\,C_n^\dagger$$

$$\rho = \begin{pmatrix} \rho_s & 0 \\ 0 & \rho_o \end{pmatrix}$$

$$H_{\rm probe} = \begin{pmatrix} h_s & 0 \\ 0 & h_o \end{pmatrix} + \frac{r^2}{2}\gamma \begin{pmatrix} 1 & 0 \\ 0 & \frac{N_c^2-2}{2(N_c^2-1)} \end{pmatrix}$$

mass shift

$$C_i^0 = \sqrt{\frac{\kappa}{N_c^2-1}}\, r^i \begin{pmatrix} 0 & 1 \\ \sqrt{N_c^2-1} & 0 \end{pmatrix},$$

$$C_i^1 = \sqrt{\frac{(N_c^2-4)\kappa}{2(N_c^2-1)}}\, r^i \begin{pmatrix} 0 & 0 \\ 0 & 1 \end{pmatrix}.$$

$$\Gamma = \kappa r^i \begin{pmatrix} 1 & 0 \\ 0 & \frac{N_c^2-2}{2(N_c^2-1)} \end{pmatrix} r^i$$

Total width → Im[V]

$$H_{\rm eff} = H_{\rm probe} - \frac{i}{2}\Gamma$$

**Six collapse operators cover**

- singlet → octet,
- octet → singlet
- octet → octet

$$\gamma \equiv \frac{g^2}{6\,N_c}\,{\rm Im}\int_{-\infty}^{+\infty} ds\,\langle T\,E^{a,i}(s,\mathbf{0})E^{a,i}(0,\mathbf{0})\rangle$$

$$\kappa \equiv \frac{g^2}{6\,N_c}\,{\rm Re}\int_{-\infty}^{+\infty} ds\,\langle T\,E^{a,i}(s,\mathbf{0})E^{a,i}(0,\mathbf{0})\rangle$$

# LO OQS + pNRQCD Hamiltonian and collapse operators

N. Brambilla, M. A. Escobedo, J. Soto and A. Vairo, 1612.07248, 1711.04515

$$\frac{d\rho_{\rm probe}}{dt} = -iH_{\rm eff}\rho_{\rm probe} + i\rho_{\rm probe}H_{\rm eff}^{\dagger} + \sum_n C_n\,\rho_{\rm probe}\,C_n^{\dagger}$$

$$\rho = \begin{pmatrix} \rho_s & 0 \\ 0 & \rho_o \end{pmatrix}$$

$$C_i^0 = \sqrt{\frac{\kappa}{N_c^2-1}}\, r^i \begin{pmatrix} 0 & 1 \\ \sqrt{N_c^2-1} & 0 \end{pmatrix},$$

$$C_i^1 = \sqrt{\frac{(N_c^2-4)\kappa}{2(N_c^2-1)}}\, r^i \begin{pmatrix} 0 & 0 \\ 0 & 1 \end{pmatrix}.$$

**Six collapse operators cover**

- singlet → octet,
- octet → singlet
- octet → octet

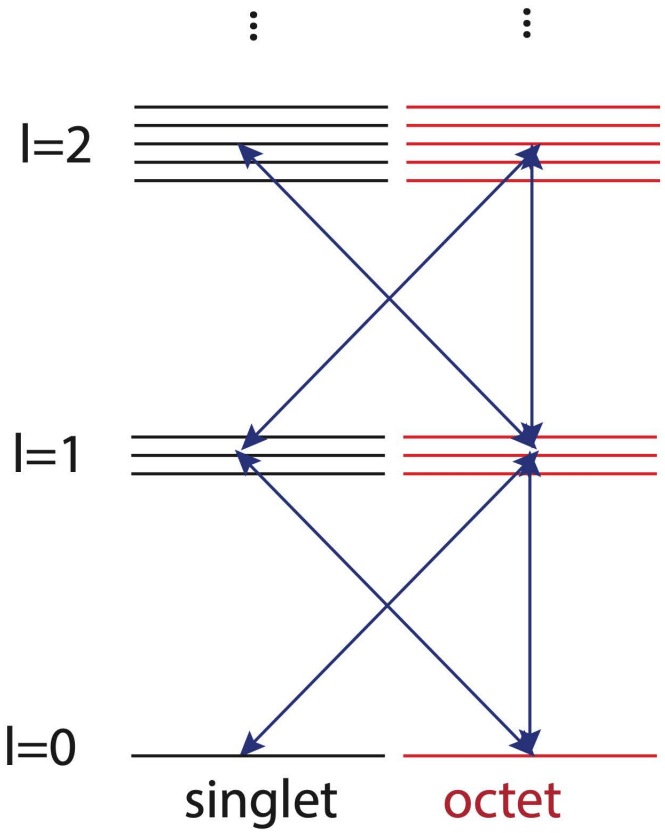

# Going beyond leading order in E/T

N. Brambilla, M.-A. Escobedo, A. Islam, M.S., A. Tiwari, A. Vairo, and P. Vander Griend, 2205.10289

- Results on previous slides were obtained by truncating at leading order (LO) in E/T (binding energy over temperature). This was extended to NLO in the reference above.

- By decomposing states into radial and angular components, for an isotropic system we can rewrite the operators as acting only on the 1d effective wavefunction
  u(r,t) = r R(r,t).

- At NLO, there are six jump operators (shown on the right).

- Based on these, one can write down the singlet and octet non-Hermitian effective Hamiltonian (see reference above for details).

$$C^{\uparrow}_{s\to o} = r - \frac{N_c\alpha_s}{8T} + \frac{1}{2MT}\left(\frac{\partial}{\partial r} - \frac{l+1}{r}\right),$$
$$C^{\downarrow}_{s\to o} = r - \frac{N_c\alpha_s}{8T} + \frac{1}{2MT}\left(\frac{\partial}{\partial r} + \frac{l}{r}\right),$$
$$C^{\uparrow}_{o\to s} = r + \frac{N_c\alpha_s}{8T} + \frac{1}{2MT}\left(\frac{\partial}{\partial r} - \frac{l+1}{r}\right),$$
$$C^{\downarrow}_{o\to s} = r + \frac{N_c\alpha_s}{8T} + \frac{1}{2MT}\left(\frac{\partial}{\partial r} + \frac{l}{r}\right),$$
$$C^{\uparrow}_{o\to o} = r + \frac{1}{2MT}\left(\frac{\partial}{\partial r} - \frac{l+1}{r}\right),$$
$$C^{\downarrow}_{o\to o} = r + \frac{1}{2MT}\left(\frac{\partial}{\partial r} + \frac{l}{r}\right).$$

# Full NLO effective Hamiltonian

The effective Hamiltonian for singlet and octet evolution is defined by $H^{\rm eff}_{s,o} = h_{s,o} + {\rm Im}(\Sigma_{s,o}) - i\Gamma_{s,o}/2$ with $\Gamma_s = \sum_{i\in\{\uparrow,\downarrow\}} \Gamma^i_{s\to o}$ and $\Gamma_o = \sum_{i\in\{\uparrow,\downarrow\}} (\Gamma^i_{o\to s} + \Gamma^i_{o\to o})$. When expressed as operators acting on the reduced wave function, the singlet effective Hamiltonian $\overline{H}^{\rm eff}_s$ is given by

$$ {\rm Re}[\overline{H}^{\rm eff}_s] = \frac{\overline{\mathcal{D}}^2}{M} - \frac{C_f\,\alpha_{\rm s}}{r} + \frac{\hat{\gamma}T^3}{2} r^2 + \frac{\hat{\kappa}T^2}{4M}\{r, p_r\}\,, \tag{3.12} $$

$$ {\rm Im}[\overline{H}^{\rm eff}_s] = -\frac{\hat{\kappa}T^3}{2}\left[\left(r - \frac{N_c\alpha_{\rm s}}{8T}\right)^2 - \frac{3}{2MT} + \frac{\overline{\mathcal{D}}^2}{(2MT)^2} + \frac{1}{2MT}\left(\frac{N_c\alpha_{\rm s}}{4T}\right)\frac{1}{r}\right], \tag{3.13} $$

where $p_r = -i\partial_r$. Similarly, the octet effective Hamiltonian $\overline{H}^{\rm eff}_o$ is given by

$$ {\rm Re}[\overline{H}^{\rm eff}_o] = \frac{\overline{\mathcal{D}}^2}{M} + \frac{1}{2N_c}\frac{\alpha_{\rm s}}{r} + \frac{N_c^2-2}{2(N_c^2-1)}\left[\frac{\hat{\gamma}T^3}{2} r^2 + \frac{\hat{\kappa}T^2}{4M}\{r, p_r\}\right], \tag{3.14} $$

$$ \begin{aligned} {\rm Im}[\overline{H}^{\rm eff}_o] = &-\frac{\hat{\kappa}T^3}{2(N_c^2-1)}\left[\left(r + \frac{N_c\alpha_{\rm s}}{8T}\right)^2 - \frac{3}{2MT} + \frac{\overline{\mathcal{D}}^2}{(2MT)^2} - \frac{1}{2MT}\left(\frac{N_c\alpha_{\rm s}}{4T}\right)\frac{1}{r}\right] \\ &-\frac{\hat{\kappa}T^3}{4(N_c^2-1)}\left[r^2 - \frac{3}{2MT} + \frac{\overline{\mathcal{D}}^2}{(2MT)^2}\right], \end{aligned} \tag{3.15} $$

where $\hat{\kappa} = \kappa/T^3$ and $\hat{\gamma} = \gamma/T^3$.

$$ \overline{\mathcal{D}}^2 = -\frac{\partial^2}{\partial r^2} + \frac{l(l+1)}{r^2} $$



N. Brambilla, M.-A. Escobedo, A. Islam, M.S., A. Tiwari, A. Vairo, and P. Vander Griend, 2205.10289

# Values of $\hat{\kappa}$ and $\hat{\gamma}$ used

- We used NLO fits to recent lattice measurements of the heavy quark transport coefficient $\hat{\kappa} \equiv \kappa/T^3$. Note that this is related to the heavy quark diffusion constant D.
  - N. Brambilla, V. Leino, P. Petreczky, and A. Vairo, 2007.10078

N. Brambilla, V. Leino, P. Petreczky, and A. Vairo, 2007.10078

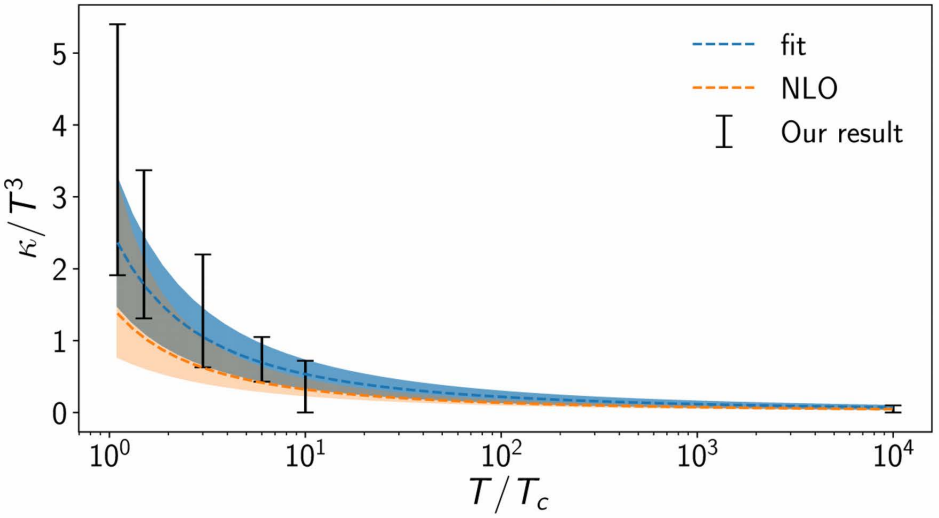


- The value of $\hat{\gamma} \equiv \gamma/T^3$ is less constrained, we vary it in the range -3.5 < $\hat{\gamma}$ < 0.
  - N. Brambilla, M. A. Escobedo, J. Soto and A. Vairo, 1612.07248.
  - N. Brambilla, M. A. Escobedo, J. Soto and A. Vairo, 1711.04515.
  - N. Brambilla, M. A. Escobedo, A. Vairo and P. Vander Griend, 1903.08063.

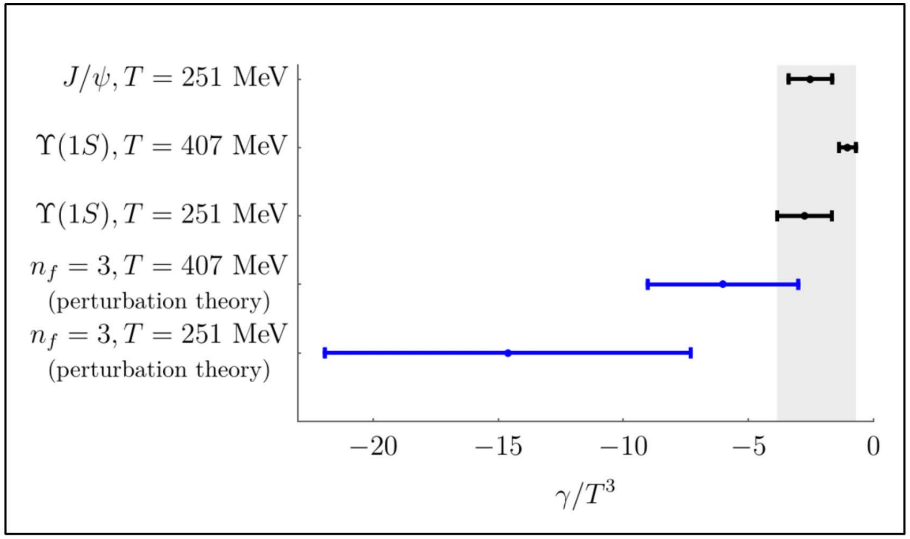


N. Brambilla, M. A. Escobedo, A. Vairo and P. Vander Griend, 1903.08063.

# Computing survival probabilities with QTraj

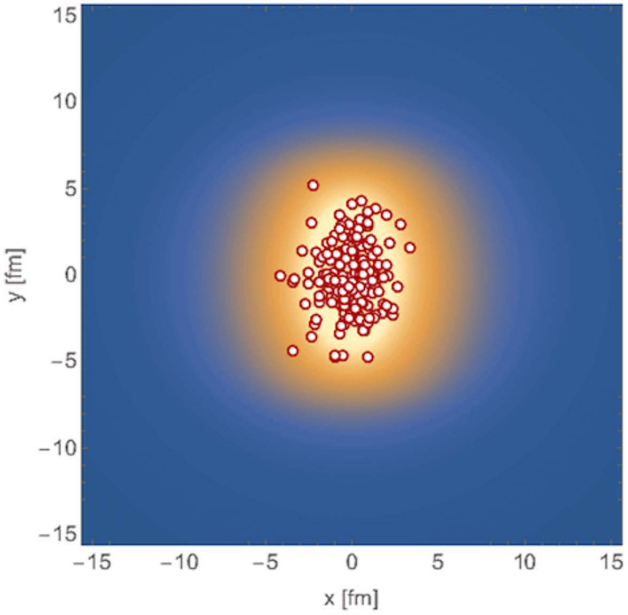


**Survival probability**

$$SP(n,l) = \frac{|\langle n,l|\psi(t_f)\rangle|^2}{|\langle n,l|\psi(t_0)\rangle|^2}$$

- Used $N = 4096$ points
- $L = 108\, a_0$
- $\Delta t = 2 \times 10^{-4}$ fm

- We sampled bottomonium production points and initial COM transverse momentum using **Monte-Carlo sampling** (physical trajectories).
- Temperature evolution provided **by 3+1D anisotropic hydrodynamics** (good description of identified soft hadron spectra and anisotropic flow, see backup slides for evidence).
- Along each physical trajectory, we solved the **real-time 3D Schrödinger equation with a complex potential and stochastically sampled jumps** → solution to Lindblad eq **(quantum trajectories algorithm)** MS et al, 2107.06147
- We then solved for the **survival probability** of S- and P-wave states (see box to the left).

# Computing survival probabilities with QTraj

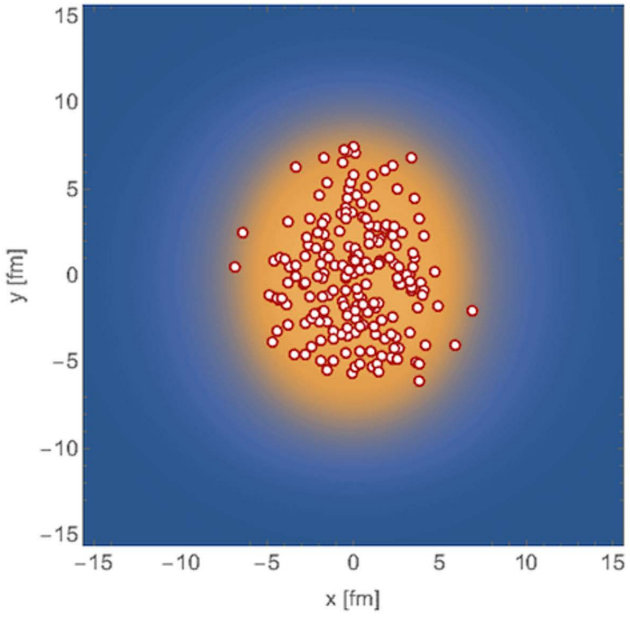


**Survival probability**

$$SP(n,l) = \frac{|\langle n,l|\psi(t_f)\rangle|^2}{|\langle n,l|\psi(t_0)\rangle|^2}$$

- Used $N = 4096$ points
- $L = 108\, a_0$
- $\Delta t = 2 \times 10^{-4}$ fm

- We sampled bottomonium production points and initial COM transverse momentum using **Monte-Carlo sampling** (physical trajectories).
- Temperature evolution provided **by 3+1D anisotropic hydrodynamics** (good description of identified soft hadron spectra and anisotropic flow, see backup slides for evidence).
- Along each physical trajectory, we solved the **real-time 3D Schrödinger equation with a complex potential and stochastically sampled jumps** → solution to Lindblad eq **(quantum trajectories algorithm)** MS et al, 2107.06147
- We then solved for the **survival probability** of S- and P-wave states (see box to the left).

# Computing survival probabilities with QTraj

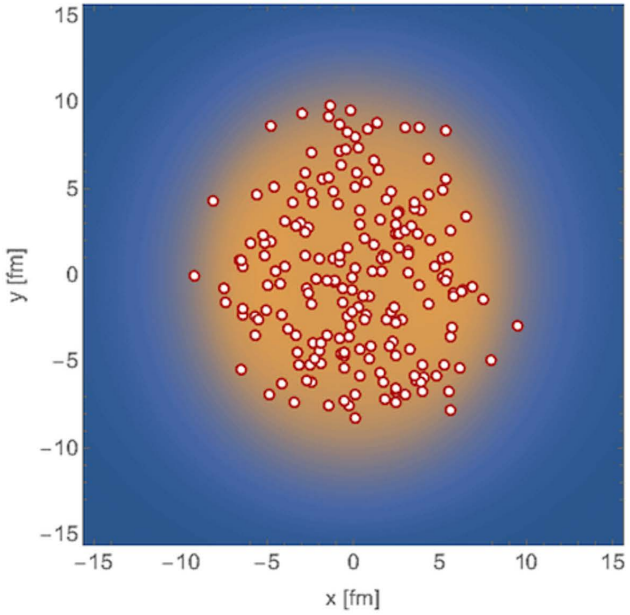


**Survival probability**

$$SP(n,l) = \frac{|\langle n,l|\psi(t_f)\rangle|^2}{|\langle n,l|\psi(t_0)\rangle|^2}$$

- Used $N = 4096$ points
- $L = 108\, a_0$
- $\Delta t = 2 \times 10^{-4}$ fm

- We sampled bottomonium production points and initial COM transverse momentum using **Monte-Carlo sampling** (physical trajectories).
- Temperature evolution provided **by 3+1D anisotropic hydrodynamics** (good description of identified soft hadron spectra and anisotropic flow, see backup slides for evidence).
- Along each physical trajectory, we solved the **real-time 3D Schrödinger equation with a complex potential and stochastically sampled jumps** → solution to Lindblad eq **(quantum trajectories algorithm)** MS et al, 2107.06147
- We then solved for the **survival probability** of S- and P-wave states (see box to the left).

# Feed-down implementation

$$\vec{N}_{\text{observed}} = F\vec{N}_{\text{direct}}$$

$$F = \begin{pmatrix} 1 & 0.2645 & 0.0194 & 0.352 & 0.18 & 0.0657 & 0.0038 & 0.1153 & 0.077 \\ 0 & 1 & 0 & 0 & 0 & 0.106 & 0.0138 & 0.181 & 0.089 \\ 0 & 0 & 1 & 0 & 0 & 0 & 0 & 0 & 0 \\ 0 & 0 & 0 & 1 & 0 & 0 & 0 & 0.0091 & 0 \\ 0 & 0 & 0 & 0 & 1 & 0 & 0 & 0 & 0.0051 \\ 0 & 0 & 0 & 0 & 0 & 1 & 0 & 0 & 0 \\ 0 & 0 & 0 & 0 & 0 & 0 & 1 & 0 & 0 \\ 0 & 0 & 0 & 0 & 0 & 0 & 0 & 1 & 0 \\ 0 & 0 & 0 & 0 & 0 & 0 & 0 & 0 & 1 \end{pmatrix}$$

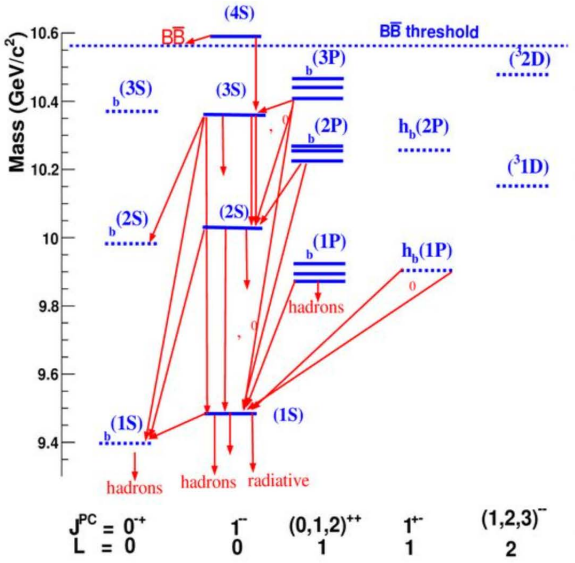


- $N_{direct}$ corresponds to $(N_{1S}, N_{2S}, N_{1P} \times 3, N_{3S}, N_{2P} \times 3, N_{2D})^T$ where, e.g., $N_{1S}$ is the final number of Y(1S) states that can decay in the dilepton channel.
- $N_{direct}$ can be obtained using $\langle N_{bin}(b) \rangle * \sigma_{direct} *$ (Survival probability)
- After feed down, we then normalize by the pp collision result scaled to AA → $R_{AA}$.

$$R^i_{AA}(c) = \frac{\left(F \cdot S(c) \cdot \vec{\sigma}_{\text{direct}}\right)^i}{\sigma^i_{\text{exp}}}$$

# NLO OQS + pNRQCD predictions for $R_{AA}$ vs $N_{part}$ at LHC

N. Brambilla, M.-A. Escobedo, A. Islam, M.S., A. Tiwari, A. Vairo, P. Vander Griend, 2205.10289

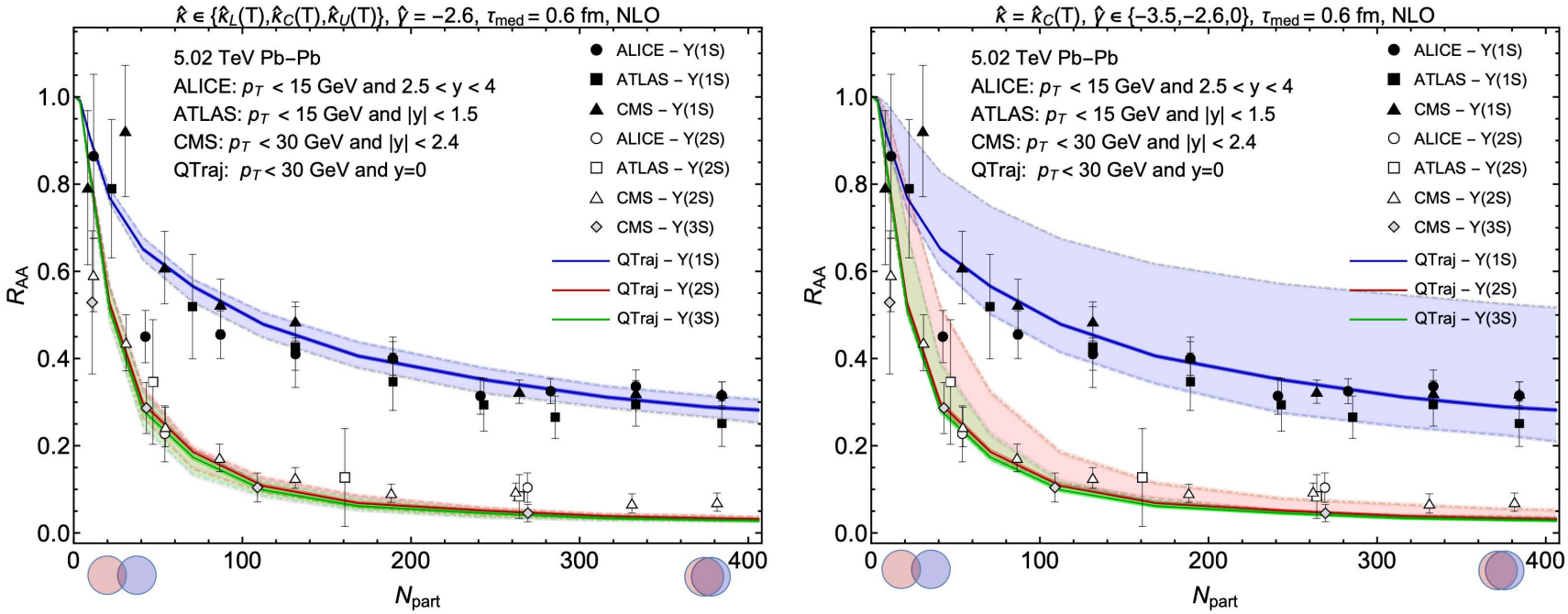


- **Left panel**: Result including feed down, when varying $\hat{\kappa}$ over the theoretical uncertainty.
- **Right panel**: Result including feed down, when varying $\hat{\gamma}$ over the theoretical uncertainty
- **Note:** The NLO results above ignore jumps ($H_{eff}$ only). The effect of jumps is expected to be small based on prior studies but requires lots of computer time (forthcoming).
- The statistical uncertainty associated with the average over physical trajectories is on the order of the line width.

# NLO $R_{AA}$ vs transverse momentum

N. Brambilla, M.-A. Escobedo, A. Islam, M.S., A. Tiwari, A. Vairo, P. Vander Griend, 2205.10289

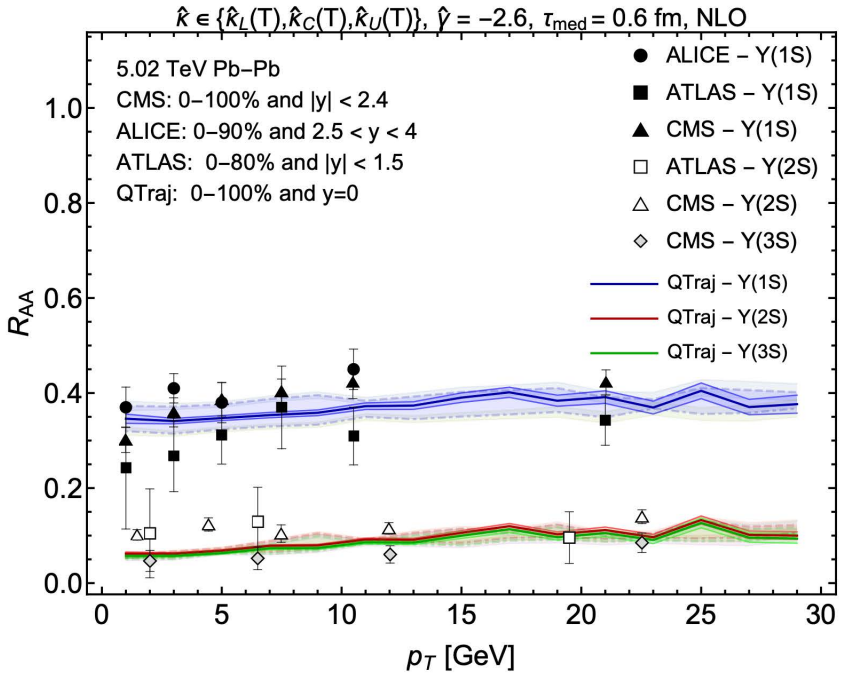


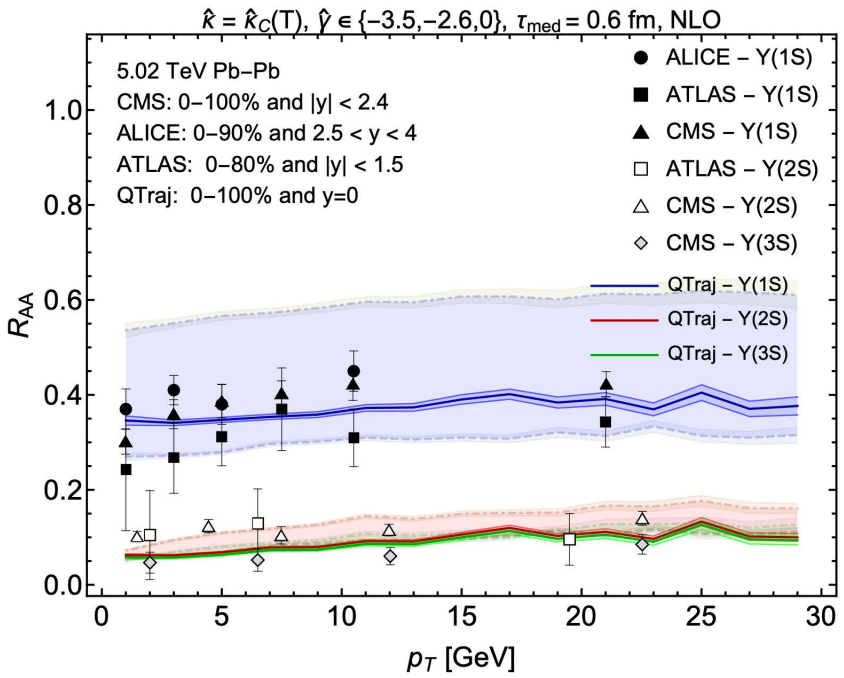


- QTraj predictions consistent with experimental observations.
- Very flat. Small decrease comes from longer time spent in the QGP as the velocity decreases.
- Once again, larger variation from uncertainty in $\hat{\gamma}$.

# Momentum-space anisotropies

4d flow tomography

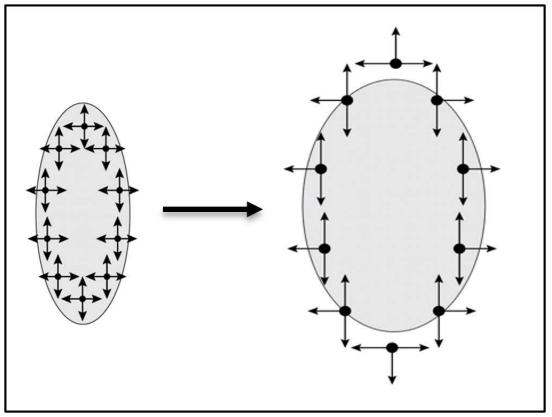

- Bottomonium probably doesn't flow in the "collective flow" sense.
- However, there can be momentum-space anisotropies induced by path-length differences in suppression along the short and long sides of the QGP.

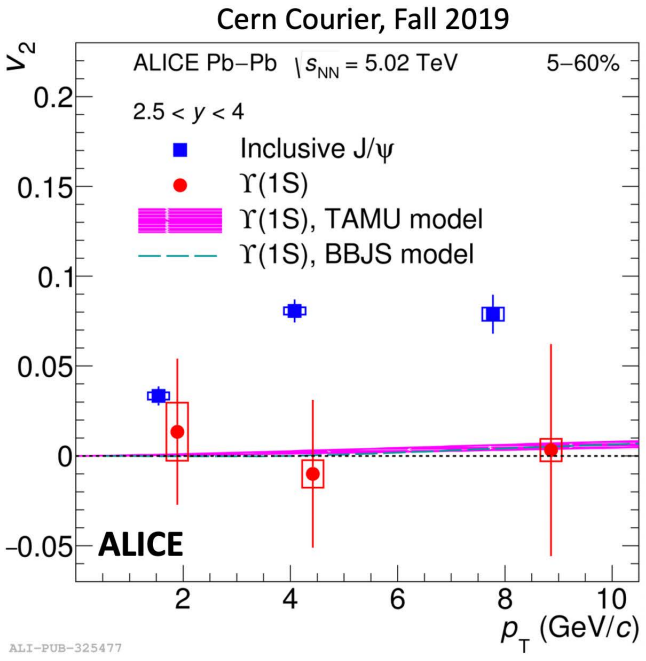


TAMU: Phys. Rev. C 96, (2017) 054901
BBJS: arXiv:1809.06235

ALICE Collaboration: arXiv:1907.03169

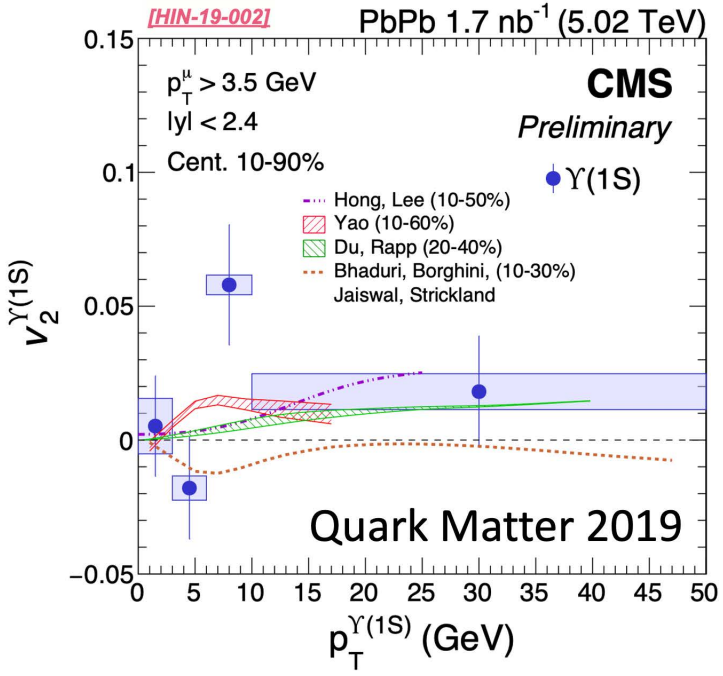

# LO Momentum-space anisotropies at LHC

N. Brambilla, M.-A. Escobedo, M.S., A. Vairo, P. Vander Griend, and J.H. Weber, 2107.06222 (Leading-Order)

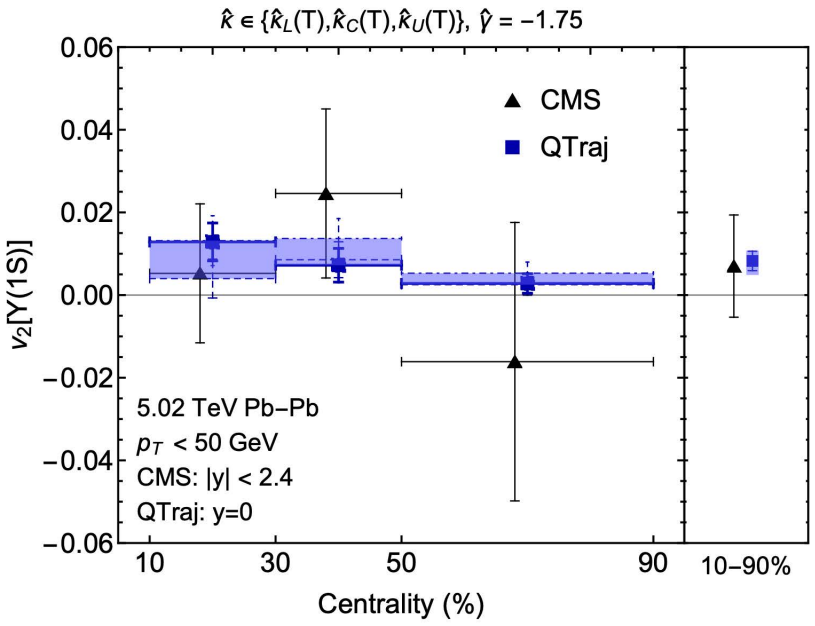


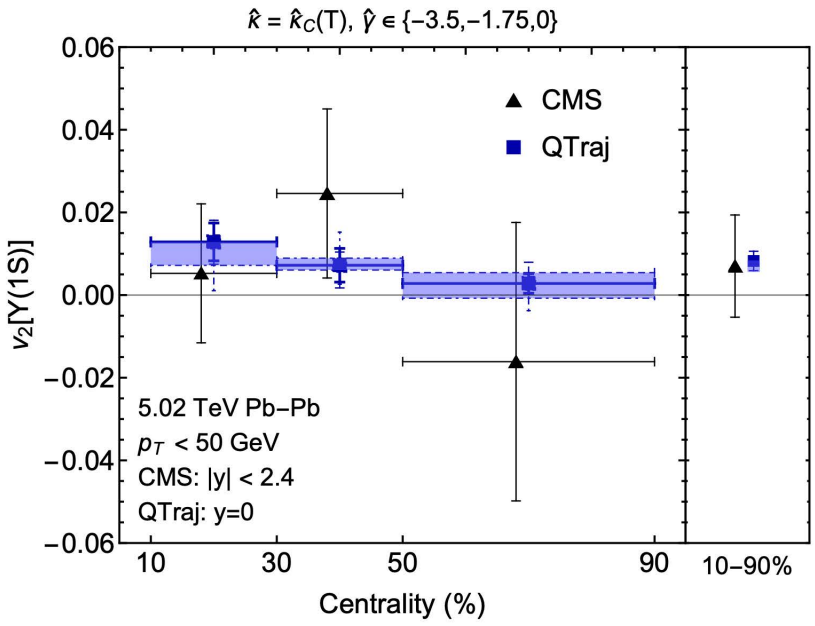


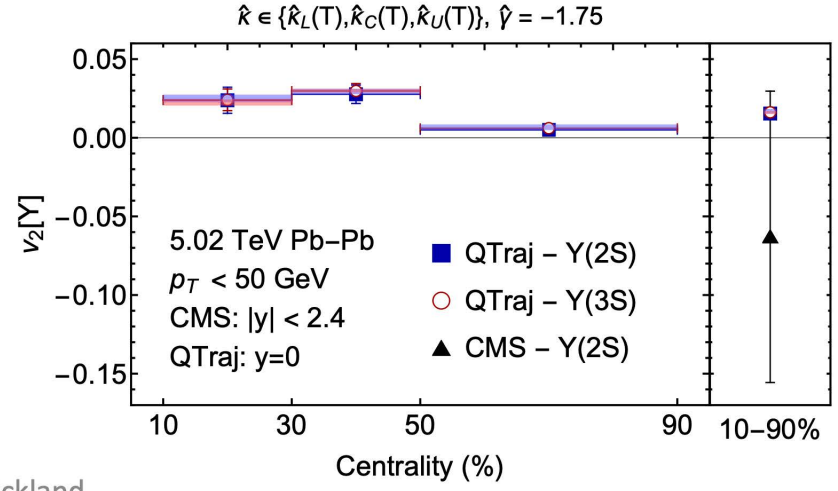


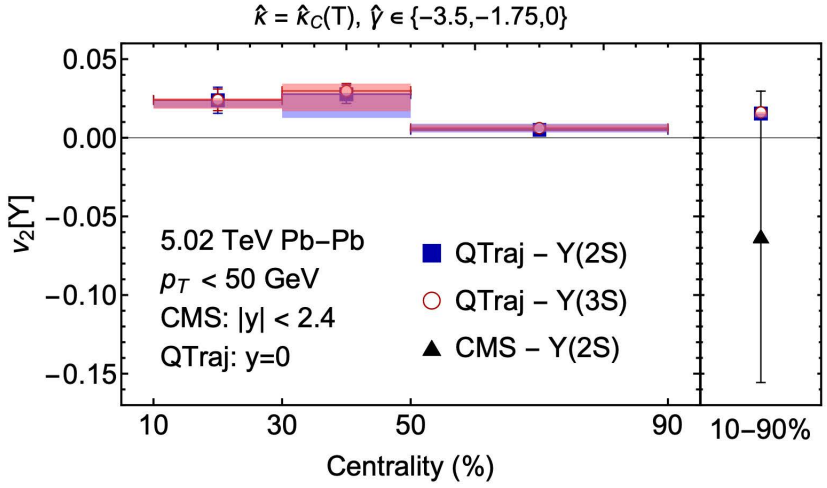

# The effect of fluctuating initial conditions

H. Alalawi, J. Boyd, C. Shen, and MS, forthcoming

- Can also study the effect of fluctuating IC hydrodynamics.
- Using MUSIC + IPGlasma tuned to 5.02 TeV Pb-Pb collisions. Both with ~ 200k physical trajectories per centrality bin
- Agrees well with aHydro results for $R_{AA}$

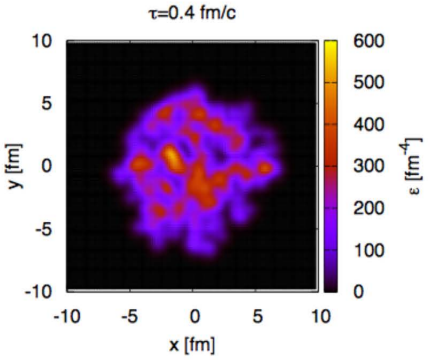


NLO + Glauber

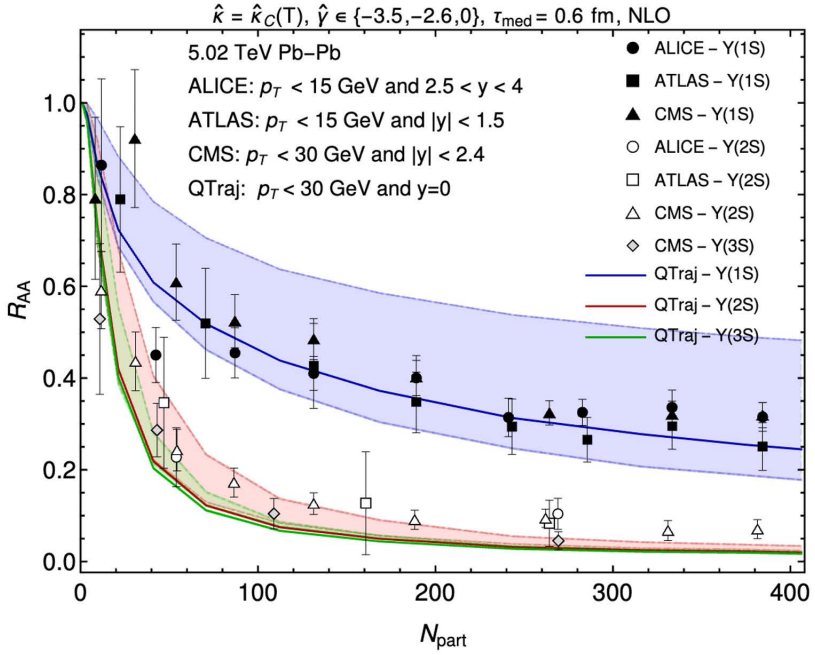


NLO + IPGlasma fluctuating ICs

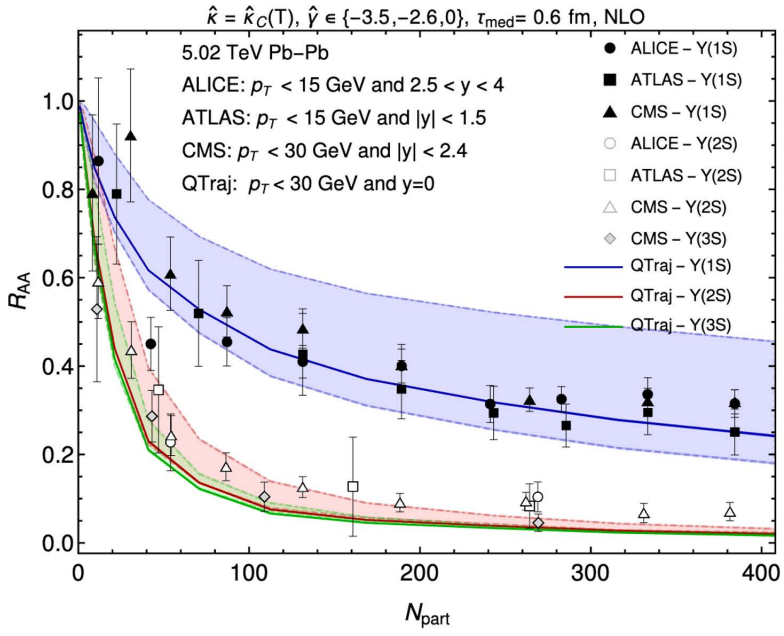

# $v_2$ with/without fluctuationing ICs

LO + Glauber

H. Alalawi, J. Boyd, C. Shen, and MS, forthcoming

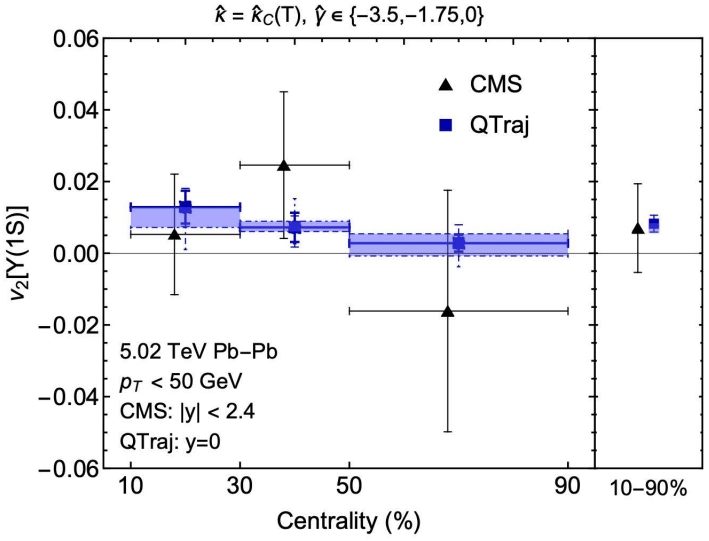


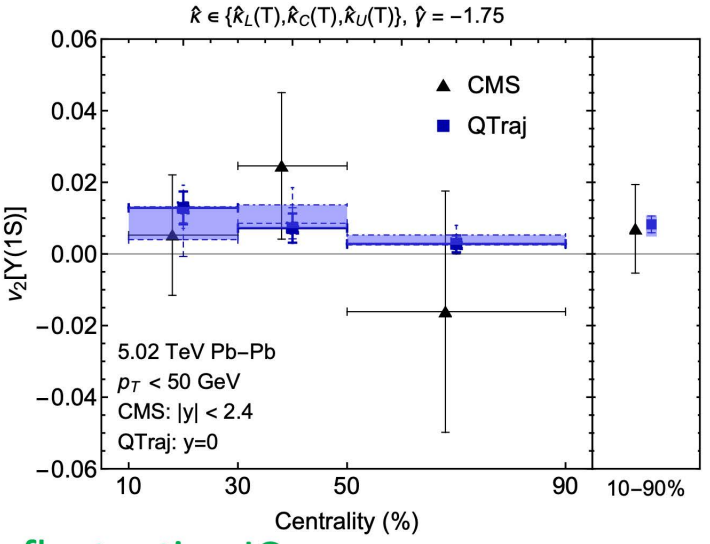


NLO + IPGlasma fluctuating ICs

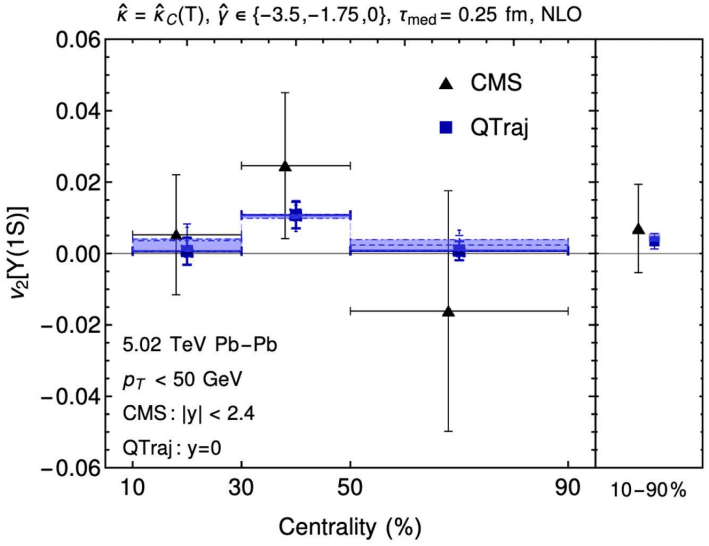


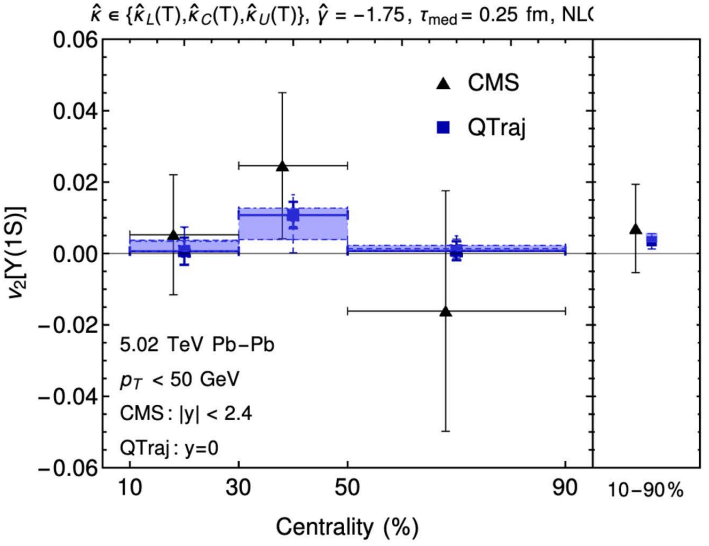

# Conclusions and Outlook

- **First 3D quantum non-abelian treatment of heavy quarkonium within the OQS+pNRQCD framework.**
- Phenomenological treatment has been extended to NLO in E/T.
- Transport coefficients used were **constrained by independent lattice measurements.**
- **OQS + pNRQCD works quite well in describing bottomonium suppression and "flow" vs $N_{\mathrm{part}}$ and $p_T$ seen at LHC energies.**
- Demonstrated that Upsilon[nS] $R_{AA}$ (and their double ratios) can provide **experimental constraints on these transport coefficients**.
- The **quantum trajectory algorithm** allows us to include effect of "**quantum jumps"** between color and angular momentum states in a **computationally scalable manner**. Code (Qtraj) has been released as an open-source package.
- Quantum jumps restore unitary of the evolution by helping to keep track of all internal state transitions, however, their final effect is small for the 1S, more important for the excited states.

# Backup slides

# A parallelizable approach: Quantum trajectories

N. Brambilla, M.-A. Escobedo, M.S., A. Vairo, P. Vander Griend, and J.H. Weber, 2012.01240

$$\frac{d\rho_{\rm probe}}{dt} = -iH_{\rm eff}\rho_{\rm probe} + i\rho_{\rm probe}H_{\rm eff}^{\dagger} + \sum_n C_n\,\rho_{\rm probe}\,C_n^{\dagger}$$

Non-unitary "no jump" evolution

Can treat this "quantum jump" term stochastically

- Can be reduced to the solution of a large set of "quantum trajectories" in which we solve a 1D Schrödinger equation with a **non-Hermitian Hamiltonian $H_{\rm eff}$**, subject to **stochastic quantum jumps**.
- The evolution with the non-Hermitian $H_{\rm eff}$ preserves the color and angular momentum state of the system (but not norm).
- Collapse/jump operators encode transitions between different color/angular momentum states (subject to selection rules).

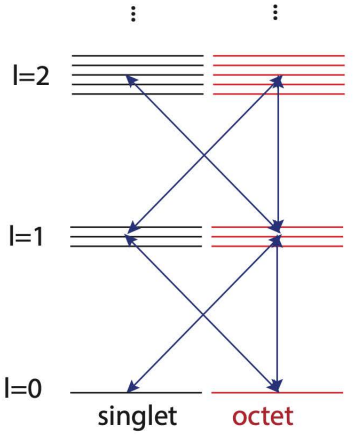


- For each **physical trajectory** (path through the QGP) we average over a large set of **independent quantum trajectories** → **Embarrassingly parallel**
- **Added benefit: Can describe all angular momentum states (no cutoff) .**

# How can one numerically solve these equations?

$$\frac{d\rho_{\rm probe}}{dt} = -iH_{\rm eff}\rho_{\rm probe} + i\rho_{\rm probe}H_{\rm eff}^{\dagger} + \sum_n C_n\,\rho_{\rm probe}\,C_n^{\dagger}$$

- Each block of the density matrix in color space can be decomposed into orbital angular momentum blockwise.
- Upon truncating in angular momentum ($l \leq l_{max}$) one can reduce both the singlet and octet blocks of the reduced density matrix to size $(l_{max}+1)^2$.
- One can then discretize the radial wavefunction ($N$ = # of lattice points) and evolve the reduced density matrix using standard differential equation and matrix solvers gives $\sim N^2(l_{max}+1)^2$ matrix size.
- **Need to describe bound and unbound states with highly localized initial wave function, so the box must be large and have small lattice spacing → large $N$ and large $l_{max}$.**
- As $N$ and $l_{max}$ become large, **the computation becomes very challenging**.
- **Need a better/faster method which we can easily parallelize.**

# NLO OQS + pNRQCD predictions for $R_{AA}$ vs $N_{part}$ at LHC

N. Brambilla, M.-A. Escobedo, A. Islam, M.S., A. Tiwari, A. Vairo, P. Vander Griend, 2205.10289

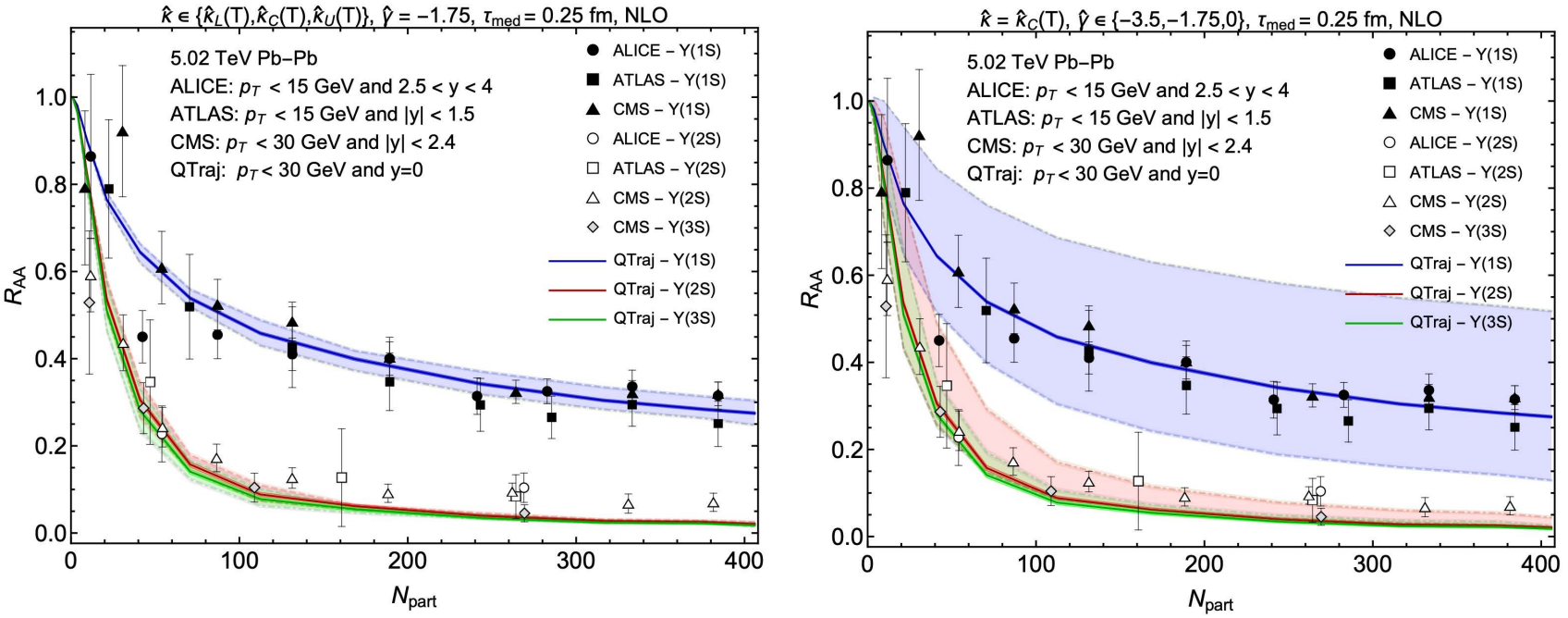


- Note that It is possible to use a shorter medium initialization time and obtain a similar description of the data.
- Above shows results using $\tau_{med}$ = 0.25 fm rather than 0.6 fm
- In this case, I changed the central value of gamma plotted, but the range of variation is the same.

# 3+1D hydrodynamical background

## Identified particle spectra

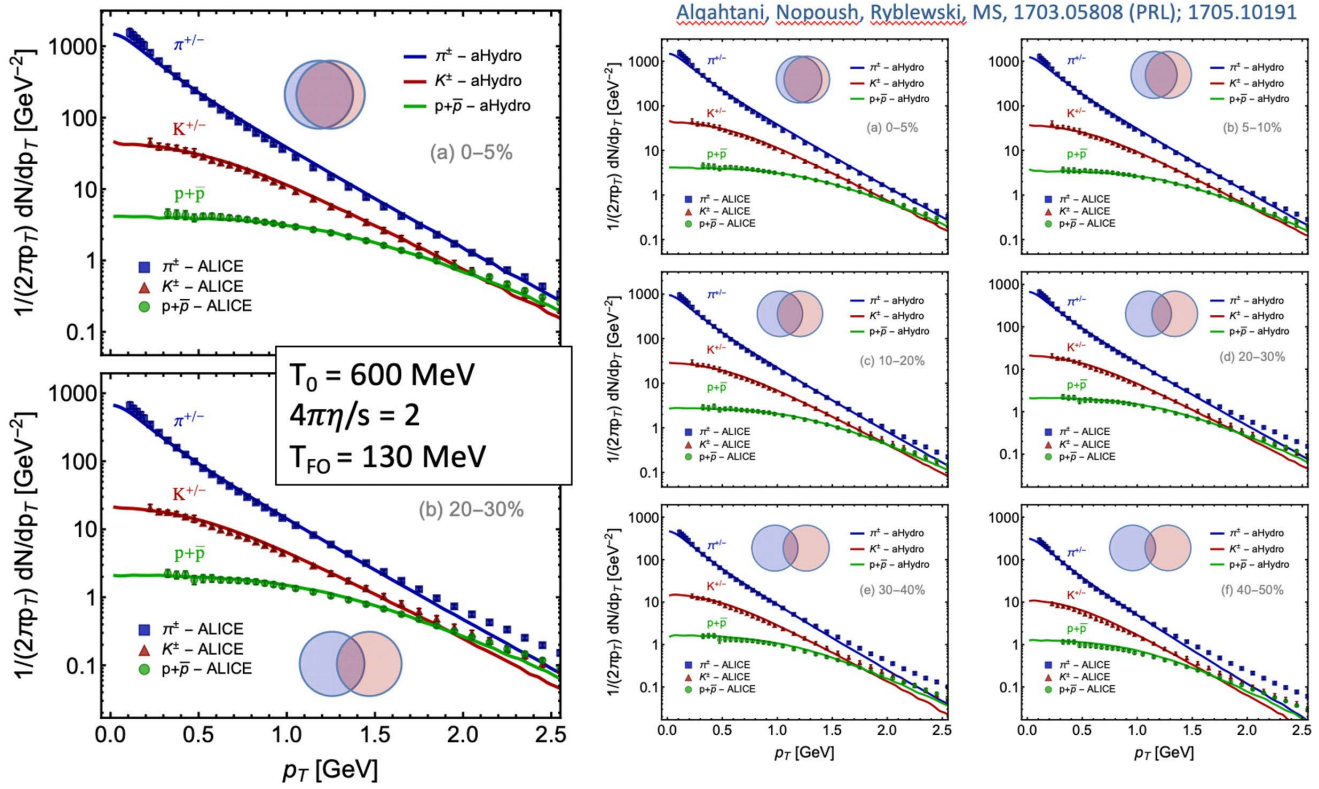


M. Strickland

Data are from the ALICE collaboration data for **Pb-Pb collisions @ 2.76 TeV/nucleon**

6

- We use a 3+1D dissipative code for the hydro background (**quasiparticle anisotropic hydrodynamics**)
- Has been tuned to RHIC and LHC heavy ion collisions
- Reproduces spectra, multiplicities, charged and identified elliptic flow of light hadrons, HBT radii, etc.

For 5.02 TeV, $T_0$ = 630 MeV @ $t_0$ = 0.25 fm/c

# Charged particle multiplicity

Alqahtani, Nopoush, Ryblewski, MS, 1703.05808; 1705.10191

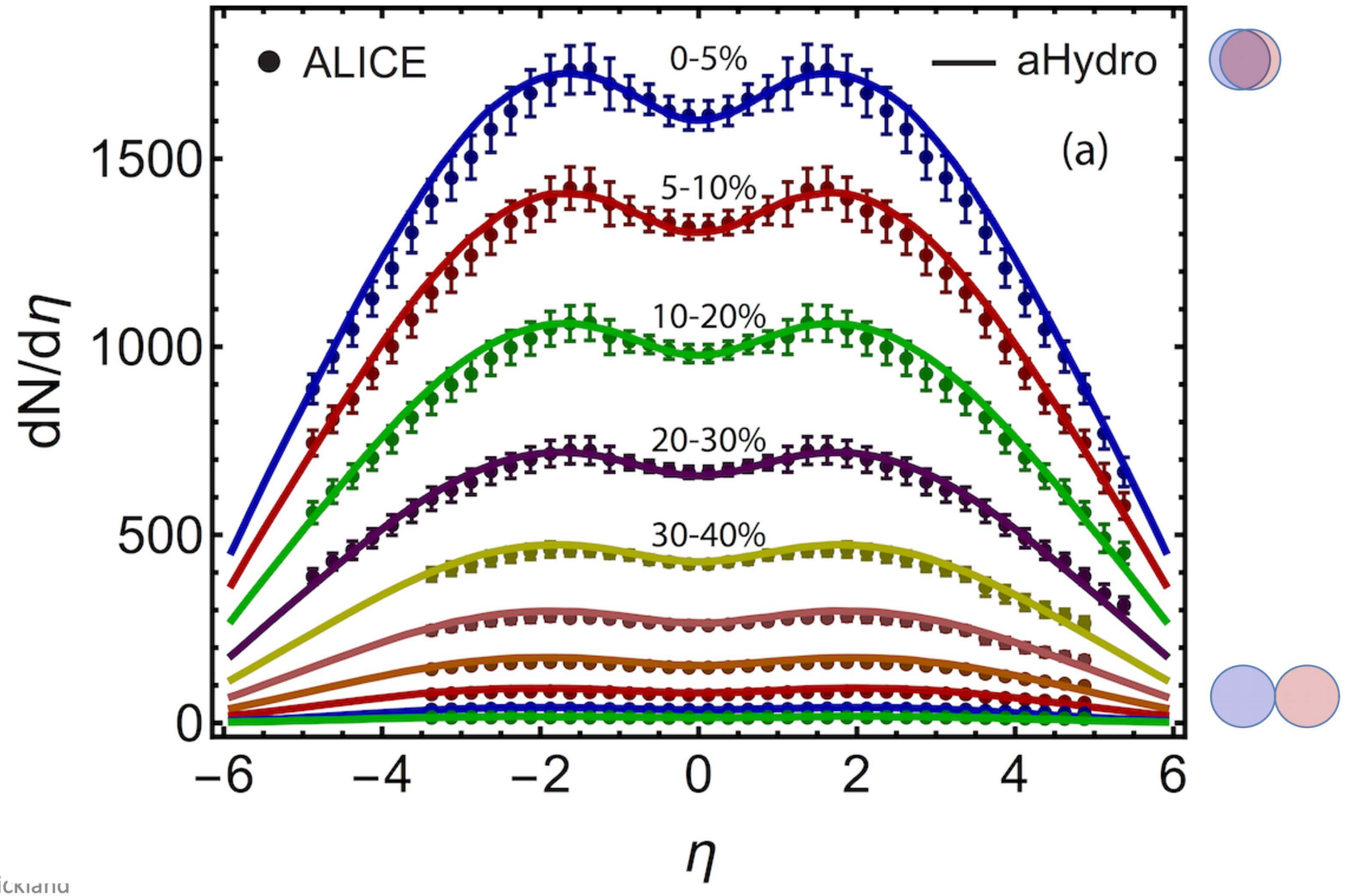

# Light hadron elliptic flow

- Quite good description of identified particle elliptic flow as well
- Central collisions → need to include fluctuating init. Conditions!

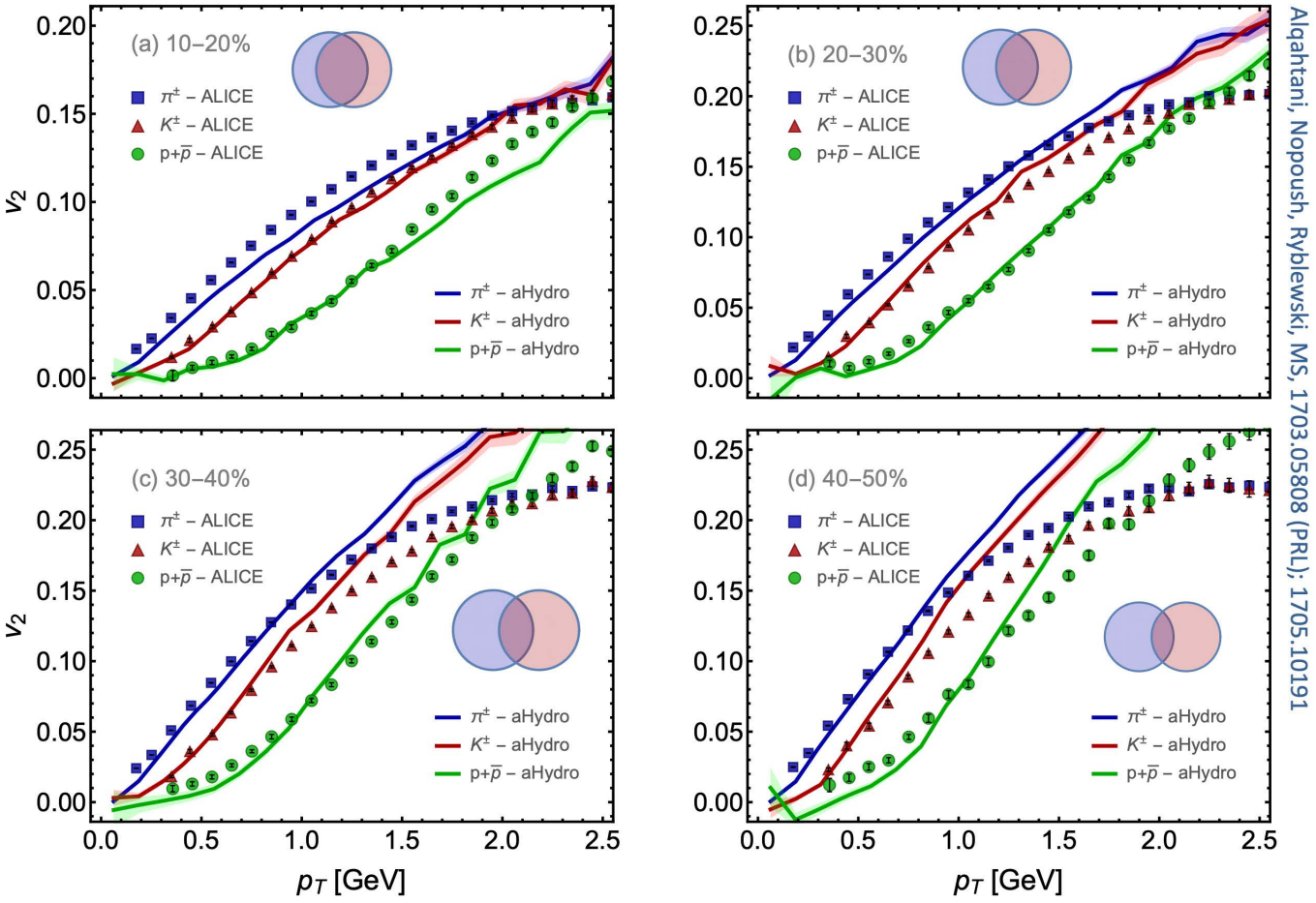

# Pionic HBT Radii

Alqahtani, Nopoush, Ryblewski, MS, 1705.10191

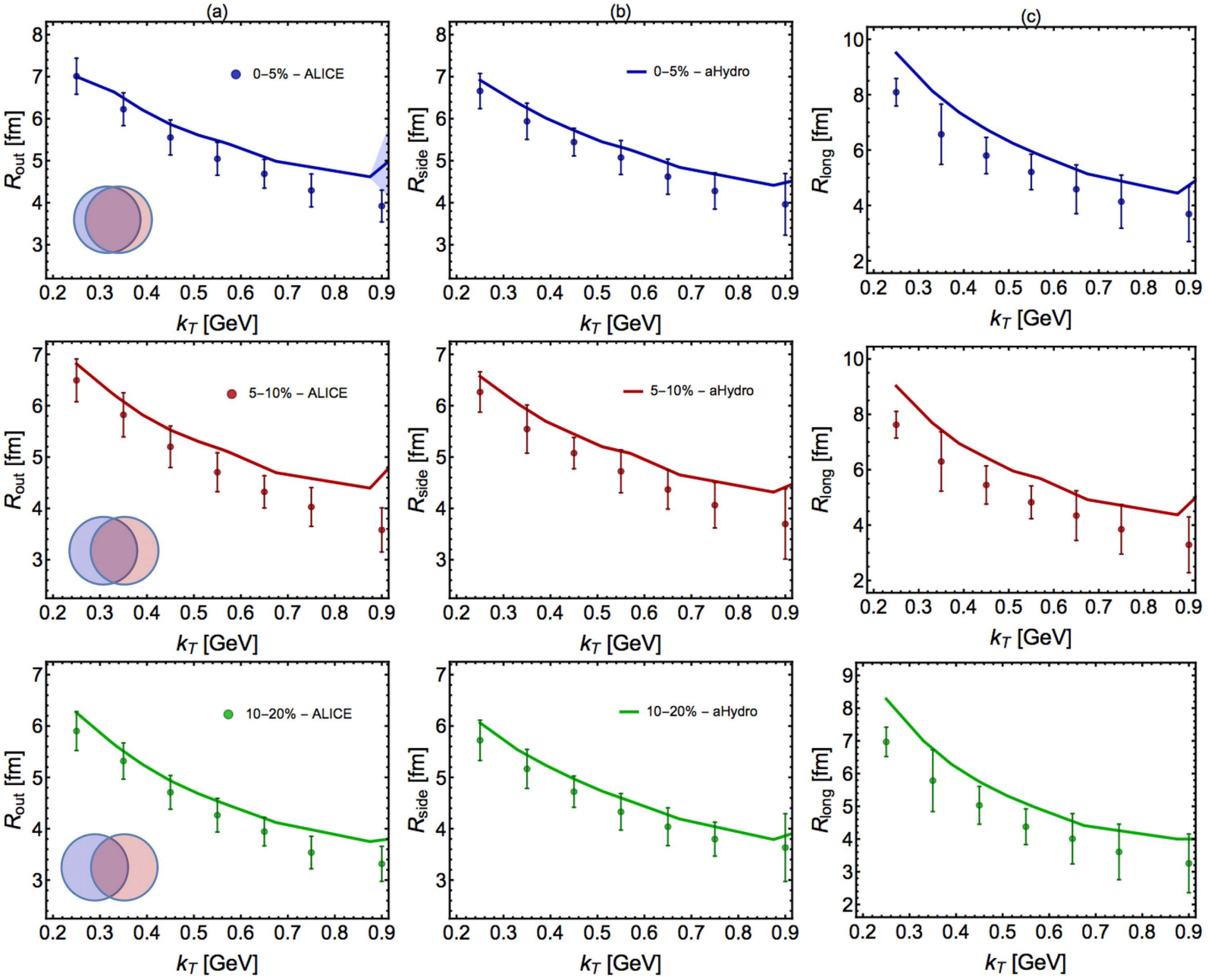

# Pionic HBT Radii Ratios

Alqahtani, Nopoush, Ryblewski, MS, 1705.10191

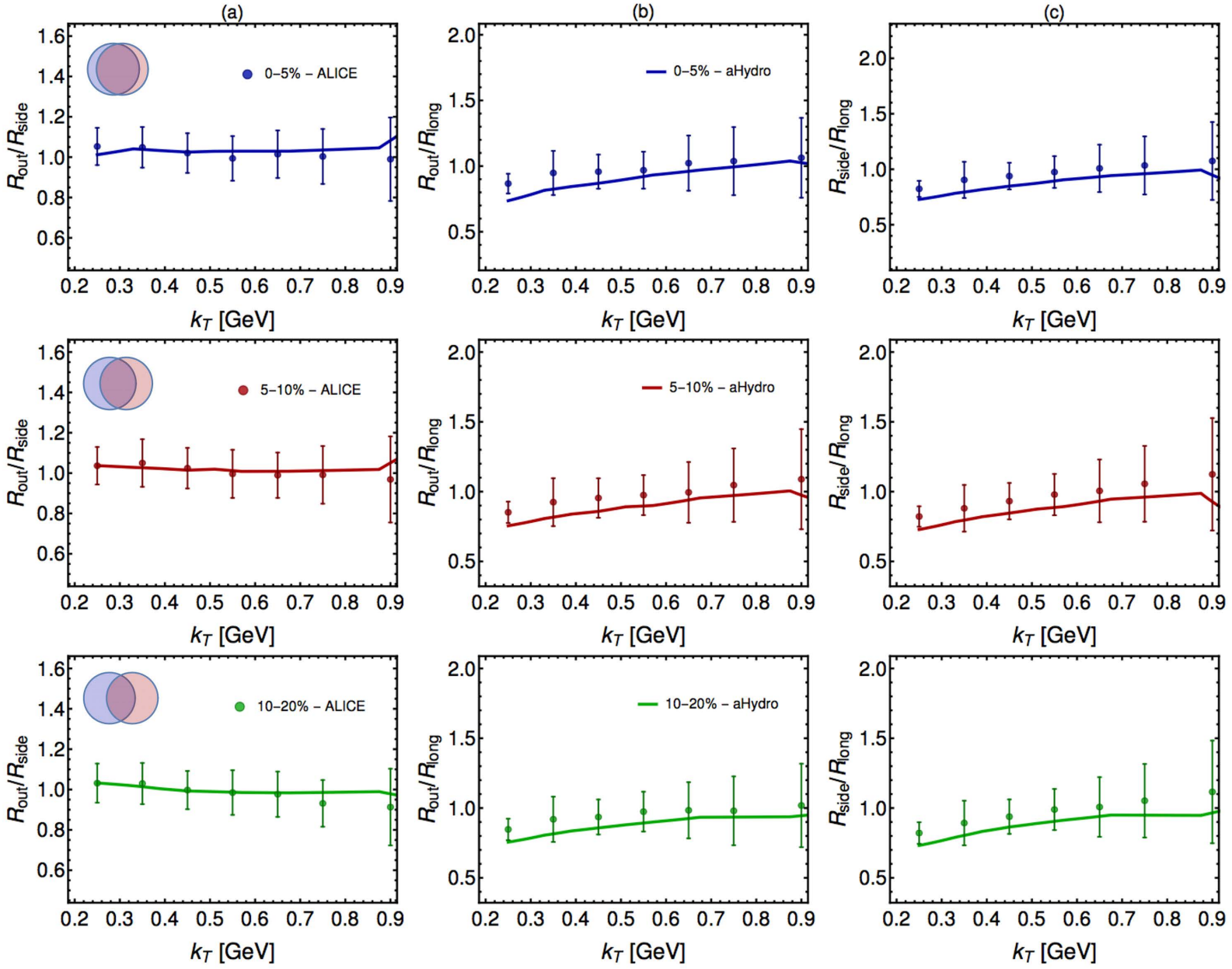

# Non-Relativistic QCD (NRQCD)

Caswell and Lepage (1986), Bodwin, Braaten and Lepage (1994)

$$\mathcal{L}_{NRQCD} = \mathcal{L}_g + \mathcal{L}_q + \mathcal{L}_\psi + \mathcal{L}_\chi + \mathcal{L}_{\psi\chi}$$

$$\mathcal{L}_g = -\frac{1}{4}F^a_{\mu\nu}F^{\mu\nu a} + \frac{d_2}{m_Q^2}F^a_{\mu\nu}D^2F^{\mu\nu a} + d_g^3\frac{1}{m_Q^2}gf_{abc}F^a_{\mu\nu}F^{\mu b}_{\alpha}F^{\nu\alpha c}$$

$$\mathcal{L}_\psi = \psi^\dagger\left(iD_0 + c_2\frac{\mathrm{D}^2}{2m_Q} + c_4\frac{\mathrm{D}^4}{8m_Q^3} + c_F g\frac{\sigma\mathrm{B}}{2m_Q} + c_D g\frac{\mathrm{DE-ED}}{8m_Q^2} + ic_S g\frac{\sigma(\mathrm{D}\times\mathrm{E}-\mathrm{E}\times\mathrm{D})}{8m_Q^2}\right)\psi$$

$$\mathcal{L}_\chi = c.c\ of\ \mathcal{L}_\psi$$

$$\mathcal{L}_{\psi\chi} = \frac{f_1(^1S_0)}{m_Q^2}\psi^\dagger\chi\chi^\dagger\psi + \frac{f_1(^3S_1)}{m_Q^2}\psi^\dagger\sigma\chi\chi^\dagger\sigma\psi + \frac{f_8(^1S_0)}{m_Q^2}\psi^\dagger T^a\chi\chi^\dagger T^a\psi + \frac{f_8(^3S_1)}{m_Q^2}\psi^\dagger T^a\sigma\chi\chi^\dagger T^a\sigma\psi$$

- **Integrating out the scale $m$ can be done perturbatively** and is not affected by the presence of the medium since $m \gg \Lambda_{QCD}, T$.
- **Hard gluons**, with energy and momentum of order $m$.
- **Soft gluons**, with energy and momentum of order $mv$.
- **Potential gluons**, with energy of order $mv^2$ and momentum of order $mv$.
- **Ultrasoft gluons**, with both energy and momentum of order $mv^2$

# NRQCD → Potential NRQCD (pNRQCD)

Pineda and Soto, '97; Brambilla, Pineda, Soto, and Vairo '99, '00, '03

Degrees of freedom at scale $\frac{1}{r} = mv$ are integrated out

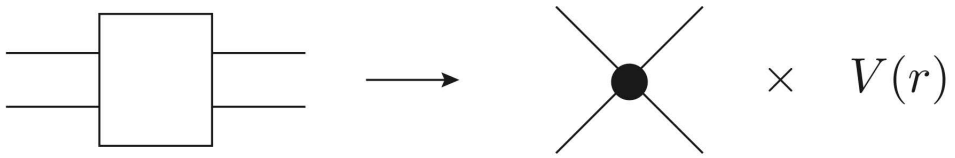

$$\times \quad V(r)$$

Power counting

$$r \sim \frac{1}{mv} \qquad t, R \sim \frac{1}{mv^2}, \frac{1}{\Lambda_{\rm QCD}}$$

Gauge fields are multiple expanded

$$A(r, R, t) = A(R, t) + \mathbf{r} \cdot \nabla A(R, t) + \dots$$

Non-analytic behavior in $r$ → matching coefficients $V$

- Resulting degrees of freedom are singlet and octet states (see Lagrangian on next slide).
- Allows to obtain manifestly gauge-invariant results.
- Easier connection lattice QCD.
- If $1/r \gg T$ we can use this as a starting point.
- In other cases, the matching between NRQCD and pNRQCD will be modified.

# NRQCD → Potential NRQCD (pNRQCD)

Pineda and Soto, '97; Brambilla, Pineda, Soto, and Vairo '99, '00, '03

$$\mathcal{L} = -\frac{1}{4} F^a_{\mu\nu} F^{\mu\nu,a} + \mathrm{Tr}\left\{ S^\dagger \left( i\partial_0 - \frac{\mathbf{p}^2}{m} - V_s \right) S + O^\dagger \left( i\partial_0 - \frac{\mathbf{p}^2}{m} - V_o \right) O \right\}$$

$$+ V_A \,\mathrm{Tr}\left\{ O^\dagger\, \mathbf{r}\cdot g\mathbf{E}\, S + S^\dagger\, \mathbf{r}\cdot g\mathbf{E}\, O \right\} \rightarrow$$

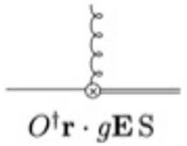


$$+ \frac{V_B}{2} \mathrm{Tr}\left\{ O^\dagger\, \mathbf{r}\cdot g\mathbf{E}\, O + O^\dagger O\, \mathbf{r}\cdot g\mathbf{E} \right\} \rightarrow$$

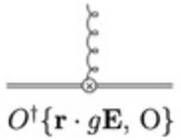


**Singlet and octet potentials**

$$V_s(r) = -C_F \frac{\alpha_s}{r}$$

$$V_o(r) = \frac{\alpha_s}{2N_c r}$$

- Based on this Lagrangian, we can perform first-principles calculations.
- Right figure shows diagrams contributing to singlet and octet self-energies.
- These enter into the calculation of Lindblad/collapse/jump operators.

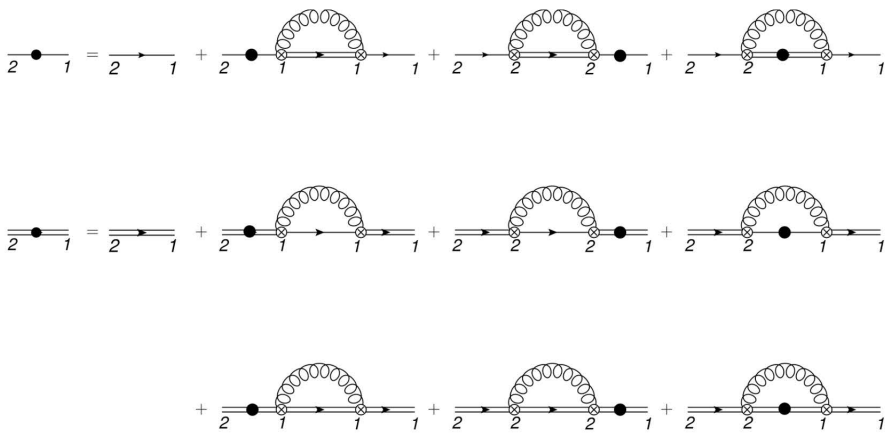

# Initial bottomonium wavefunction

- We took the initial wavefunction to be given by a smeared delta function (local production due to large mass, $\Delta \sim 1/M$) of the form

$$u_\ell(r, \tau = 0) \propto r^{\ell+1} \exp(-r^2/\Delta^2)$$

- For a given $l$, the **initial state is a quantum linear superposition** of the eigenstates of H.
- **Includes both bound and unbound states.**
- We took $\Delta = 0.2\ a_0$ which reproduces results obtained with a true delta to within 1%.

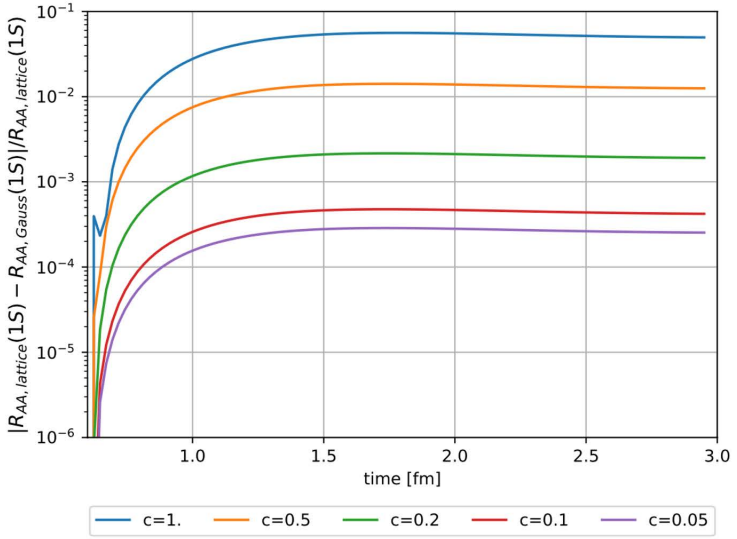


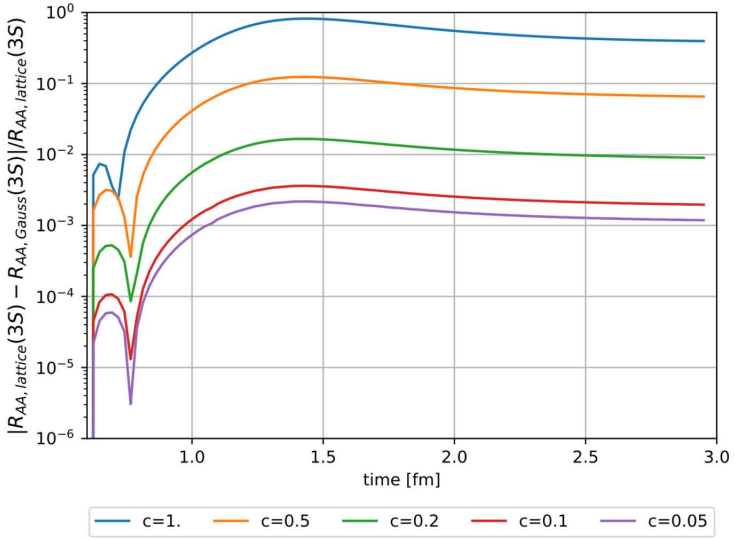

# Heuristic understanding – Noisy QM

- Heavy quark bound states have an in-medium potential with both real and imaginary parts. This results in a large in-medium width.
- How can we understand the emergence of the imaginary part in a simple manner in an intuitive manner?
- **Consider a non-relativistic bound state subject to a noisy potential**

$$H(\mathbf{r},t) = -\frac{\nabla_{\mathbf{r}}^2}{M} + V(\mathbf{r}) + \Theta(\mathbf{r},t)$$

$$\Theta(\mathbf{r},t) = \theta\left(\mathbf{R}+\frac{\mathbf{r}}{2},t\right) - \theta\left(\mathbf{R}-\frac{\mathbf{r}}{2},t\right)$$

Noise due to environment (assumed here to be color neutral).

- Noise has zero mean, is uncorrelated in time, and has a spatial correlation function $D(\boldsymbol{r})$

$$\langle\theta(\mathbf{x},t)\rangle = 0 \qquad \langle\theta(\mathbf{x},t)\theta(\mathbf{x}',t')\rangle = D(\mathbf{x}-\mathbf{x}')\delta(t-t')$$

**Note:** The treatment presented here does not include possibility of color-charged noise, more on this coming …

# Heuristic understanding – Noisy QM

- Expanding the time evolution operator up to $O(\Delta t^{3/2})$

$$e^{-i\Delta t\, H(\mathbf{r},t)} \simeq 1 - i\Delta t\, H(\mathbf{r},t) - \frac{1}{2}\left\{\Delta t\, H(\mathbf{r},t)\right\}^2 + \ldots$$

$$\approx 1 - i\Delta t\left[H(\mathbf{r},t) - \frac{i}{2}\Delta t\left\{\theta(\mathbf{x},t)^2 + \theta(\mathbf{x}',t)^2 - 2\,\theta(\mathbf{x},t)\theta(\mathbf{x}',t)\right\}\right]$$

- Now construct an effective Hamiltonian that is averaged over the noise

$$\langle \mathrm{H}_{\mathrm{eff}}(\mathbf{r},t)\rangle \simeq H(\mathbf{r},t) - \frac{i}{2}\Delta t\left\{\langle\theta(\mathbf{x},t)^2\rangle + \langle\theta(\mathbf{x}',t)^2\rangle - 2\,\langle\theta(\mathbf{x},t)\theta(\mathbf{x}',t)\rangle\right\}$$

Imaginary part of the potential

$$\langle \mathrm{H}_{\mathrm{eff}}(\mathbf{r},t)\rangle = -\frac{\nabla^2_{\mathbf{r}}}{M} + V(\mathbf{r}) - i\left\{D(\mathbf{0}) - D(\mathbf{r})\right\}$$

$$\Im[V(r)] = D(\mathbf{r}) - D(\mathbf{0})$$

Imaginary part emerges through interference of wave function with itself when summing over environmental noise.